

Floquet Control of Electron and Exciton Transport in Kekulé-Distorted Graphene

Sita Kandel^{1,2} and Godfrey Gumbs^{1,2}

¹*Department of Physics, Hunter College, City University of New York,
695 Park Avenue, New York, NY 10065 USA and*

²*The Graduate School and University Center, The City University of New York, New York, NY 10016, USA*

(Dated: February 12, 2026)

This work investigates the Floquet dynamics of electrons and excitons (particle-hole pairs) in a Dirac material referred to as Kekulé-distorted graphene. Specifically, we examine the role played by a high frequency driving electromagnetic field on the tunneling and blocking by a potential barrier on both the charged single particles as well as the neutral composite particles. We demonstrate that the small effective masses of the electron and hole for the energy spectrum of this Kekulé distorted graphene leads to practically almost perfect transmission across a symmetric potential barrier for any angle of incidence of impinging excitons. However, this unexpected Klein paradox for excitons does not hold for the single-particle electrons. The reduced total transmission of electron due to Kekulé distortion is more suppressed due to irradiation. Additionally, we calculate and investigate the exciton binding energy since the quantum tunneling of a bound electron-hole pair across a potential barrier is governed by its mass measured in the center of mass and binding energy of the composite pair. Thus, irradiation with circularly polarized light fundamentally modifies exciton formation, coherence and transport properties, thereby producing unusual topological behaviors. These behaviors are unlike conventional Dirac materials. Possible technical applications of the results arising from our investigation include valleytronics due to the folding of the valleys, thereby making intervalley coupling feasible. Other practical applications include optoelectronics due to Floquet tuning of energy spectrum and transport properties.

Keywords: Floquet driven energy spectrum, tunneling and blocking of a beam of electrons and particle-hole pairs across a barrier, Klein tunneling.

I. INTRODUCTION

In recent times, spatially inhomogeneous two dimensional (2D) materials have been attracting significant scrutiny due to their potential usage to display novel physical phenomena^{1–6}. Kekulé-distorted graphene^{7–13} is one of the most galvanizing materials among these low-dimensional materials. With arbitrary periodic perturbation on Kekulé-distorted graphen, the two nonequivalent Dirac cones at K^\pm which are subject to time-reversal symmetry at the corners of a corresponding hexagonal Brillouin zone like graphene are folded at the center Γ point of the new hexagonal superlattice Brillouin zone, resulting in either a gap (Kek-O) or the superposition of two cones with different Fermi velocities (Kek-Y)^{7–9}. The Kekulé-phase was first reported in graphene sheets epitaxially grown over copper substrates¹⁴ and also in monolayer graphene on top of silicon oxide¹⁵. After the experimental realization, several works have been reported exploring the physical^{7,15} electronic⁸, optical^{11,12}, transport¹⁶ and several more intriguing properties^{17–20} including spin-orbit interaction,²¹ as well as phonon²² or magnon^{23,24} excitations. Recently, direct experimental evidence for chiral symmetry breaking in a Li-intercalated Kekulé-ordered graphene from both electron spectroscopic and microscopic measurements have been reported.¹³

In this work, we consider the Y-shaped Kek lattice as schematically exhibited in Fig. 1, where one of six carbon atoms in each superlattice unit cell display three shorter nearest-neighbor bond (green lines) shaped like the letter Y. The superlattice unit cell of the Kekulé distorted graphene is $\sqrt{3} \times \sqrt{3}$ larger than the graphene unit cell. The structure preserves inversion symmetry and two chiral valleys coupled together to form massless Dirac bands leading to vanishing valley degeneracy. We study the valley coupled tunneling of electrons in such Y-shaped Kek structure calculating the probability currents explicitly for both reflection and transmission of electrons across a potential barrier of finite height and width. By matching boundary conditions at the interface of this barrier, we acquire valley resolved reflection and transmission coefficients as functions of the incident kinetic energy and the angle of incidence, as well as the barrier height and width for chosen Kekulé parameter. Our present study reveals that the intervalley coupling enhances the perfect transmission around normal incidence for small barrier width. However, the resonant tunneling is suppressed when the barrier width is increased. We have been motivated to investigate the tunneling behavior by opening a gap between the conduction and valence bands as well as between two folded cone in such a structure.

There are many ways of modifying the band structure of Dirac like electronic system. Among them, manipulating the electronic properties by using high-frequency dressing field which is called Floquet engineering has become a very

powerful and efficient technique nowadays in the era of 2D materials^{25–30} although it is not a new concept in quantum physics. The field of Floquet engineering -where matter is coherently driven by periodic temporal perturbations- was initiated by Fistul and Efetov who proposed that a dynamically opened gap, generated by irradiating graphene with an electromagnetic field, could be employed to control Klein tunneling in a p-n junction.^{31,32} Later, Oka and Aoki recognized the nontrivial nature of this gap and predicted a light induced topological anomalous Hall state associated with an induced magnetic field due to symmetry breaking.³³ Merboldt et al.³⁴ recently revealed an experimental framework for implementing Floquet-engineering protocols in metallic and semimetallic platforms with potentially nontrivial topological characteristics. These developments motivate the exploration of periodically driven 2D semimetals such as graphene. Here, we present the effect due to high frequency circularly polarized light irradiation on band structure and tunneling behavior. The result shows that a small difference is established between the valleys and a small gap is opened between the valence and conduction energy bands. This gap opening irradiation suppresses the tunneling of electrons but still preserves the perfect transmission for head-on collision.

In gapped Kek-Y graphene, the spatially separated electrons and holes form a bound quasi particle usually referred to as excitons. Study of quantum mechanical tunneling of composite particles dates back to around the 1960's by Zakhарьев et al.^{35,36}. Ever since that time, it has become an active area of research investigation. For example, in 1964 Saito and Kayanuma³⁷ investigated the resonant tunneling of a pair of bound particles through a single potential barrier, Kavka et al.^{38–40} reported the time dependent formalism of molecular tunneling, of excitons through quantum heterostructure barrier and tunneling of molecules in three dimensions. Exciton-assisted electron tunneling in vander Waals heterostructures consisting of graphene and gold electrodes separated by hexagonal boron nitride with an adjacent TMD (transition-metal dichalcogenide) monolayer was recently published in "nature materials".⁴¹ Similarly, exciton-assisted resonant tunneling has been observed in conventional semiconductor quantum wells.^{42,43} In this respect, tunneling of excitons in gapped Kek-Y graphene across a finite width square potential barrier of equal strength as well as delta potential of inequivalent strength for electrons and holes becomes an interesting problem to include in this paper. We have merged together in this work the exciton binding energy and the reflection and transmission probability of an exciton since the survival of an exciton after it impinges the potential barrier is relevant in this calculation.

The remainder of this paper is organized in the following way. In Sec. II, we introduce a low-energy Hamiltonian for Kek-Y graphene and briefly review some essential properties resulting from the energy dispersion and the corresponding electronic eigenfunctions in the absence of irradiation. Section III is devoted to deriving an effective Hamiltonian which has the same stroboscopic effects as the externally applied time-dependent periodic potential employed to irradiate the system with elliptically polarized light. We also analyze the electron-photon dressed states under this irradiation. In Sec. IV(A), we calculate the probability current, transmission and reflection probability of a particle incident on the potential barrier and observe the valley resolved Klein tunneling in the absence of irradiation. With help from the derived transmission probability, we obtain numerically the quantum conductivity through a monolayer of Kek-Y distorted graphene. Our results for the effect of circularly polarized irradiation on transmission and reflection are presented in Sec. IV(B). Tunneling of excitons on irradiated gap-induced Kek-Y graphene is calculated and analyzed in Sec. V. The final conclusions of our presented results and outlook are presented in Sec. VI and the Appendix includes the steps and lengthy expressions behind some complicated mathematical calculations.

II. LOW-ENERGY HAMILTONIAN AND ENERGY EIGENSTATES FOR KEK-Y GRAPHENE

First, to establish notation, we briefly review the electronic band structure and eigenfunctions in Kek-Y distorted graphene. For this type of distortion, the Dirac cones will fold on each other, as shown in Fig. 1, which results in two Dirac cones with one buried inside the other with no bandgap, but with different Fermi velocities.

The low-energy Hamiltonian for Kek-Y graphene can be expressed as^{11,44}

$$\hat{\mathcal{H}}_Y(\mathbf{k} | \Delta_0) = \hbar v_F \hat{\mathcal{T}}_0^{(2)} \otimes \left(\mathbf{k} \cdot \hat{\boldsymbol{\Sigma}}^{(2)} \right) + \hbar v_F \Delta_0 \left(\mathbf{k} \cdot \hat{\boldsymbol{\tau}}^{(2)} \right) \otimes \hat{\Sigma}_0^{(2)}, \quad (1)$$

where $\mathbf{k} = \{k_x, k_y\}$ is a wave vector of electrons, v_F is the Fermi velocity in regular unstrained graphene and Δ_0 is a dimensionless strain-induced coupling parameter. As $\Delta_0 \rightarrow 0$, we recover the Dirac Hamiltonian for pristine graphene for unfolded τ_+ and τ_- valleys, *i.e.*, retaining only the first term on the right hand side of Eq. (1). We indicate that Eq. (1) is only valid for a small strain-coupling parameter Δ_0 , and it may be modified as the strength of the strain is increased. However, in most cases, Δ_0 is assumed small in order to retain the graphene signature of the material. Here, we choose $\Delta_0 \sim 0.1$ and 0.2 in our calculations but derive a generalized model by assuming a substantial difference between two Fermi velocities $v_F(1 \pm \Delta_0)$. Additionally,

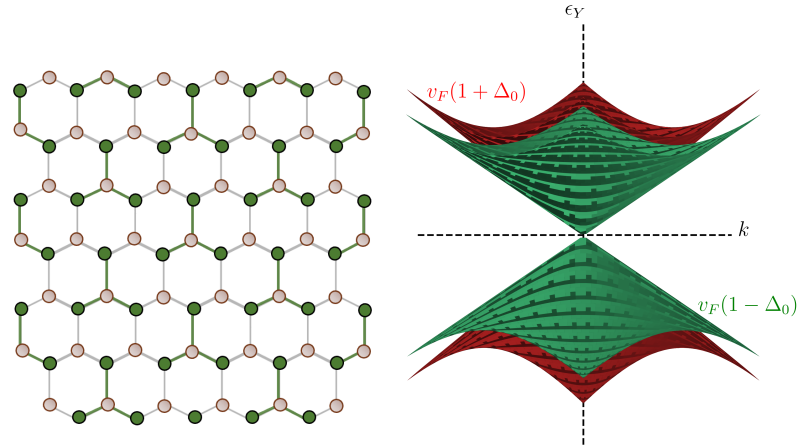


FIG. 1: (Color online) Kekulé distorted honeycomb lattice (left) and pictorial representation of two Dirac cones (right) of Kek-Y distorted graphene .

$$\hat{\Sigma}_x^{(2)} = \hat{\mathcal{T}}_x^{(2)} = \begin{pmatrix} 0 & 1 \\ 1 & 0 \end{pmatrix}, \quad (2)$$

$$\hat{\Sigma}_y^{(2)} = \hat{\mathcal{T}}_y^{(2)} = \begin{pmatrix} 0 & -i \\ i & 0 \end{pmatrix}, \quad (3)$$

which act in the spin- and pseudo-spin subspaces, respectively. Correspondingly, $\hat{\Sigma}_0^{(2)}$ and $\hat{\mathcal{T}}_0^{(2)}$ in Eq. (1) are two 2×2 unit matrices in the spin- and pseudo-spin subspaces, written as

$$\hat{\Sigma}_0^{(2)} = \hat{\mathcal{T}}_0^{(2)} = \begin{pmatrix} 1 & 0 \\ 0 & 1 \end{pmatrix}. \quad (4)$$

Equation (1) can be expressed in a simple matrix form

$$\hat{\mathcal{H}}_Y(\mathbf{k} | \Delta_0) = \hbar v_F \begin{pmatrix} \mathbf{k} \cdot \hat{\Sigma}^{(2)} & \Delta_0 (k_x - ik_y) \hat{\Sigma}_0^{(2)} \\ \Delta_0 (k_x + ik_y) \hat{\Sigma}_0^{(2)} & \mathbf{k} \cdot \hat{\Sigma}^{(2)} \end{pmatrix}, \quad (5)$$

or explicitly as

$$\hat{\mathcal{H}}_Y(\mathbf{k} | \Delta_0) = \hbar v_F \begin{pmatrix} 0 & k_x - ik_y & \Delta_0(k_x - ik_y) & 0 \\ k_x + ik_y & 0 & 0 & \Delta_0(k_x - ik_y) \\ \Delta_0(k_x + ik_y) & 0 & 0 & k_x - ik_y \\ 0 & \Delta_0(k_x + ik_y) & k_x + ik_y & 0 \end{pmatrix}. \quad (6)$$

The energy dispersions of Kekulé-Y graphene are simply obtained as eigenvalues of the matrix defined in Eq. (6), yielding

$$\varepsilon_Y(s, \tau | k, \Delta_0) = s \hbar v_F (1 + \tau \Delta_0) k, \quad (7)$$

which represent two Dirac cones with different Fermi velocities $v_F(1 \pm \Delta_0)$, as displayed in Fig. 2, where $s = \pm 1$ is a band index while $\tau = \pm 1$ corresponds to two different Fermi velocities due to strain coupling. These two types of

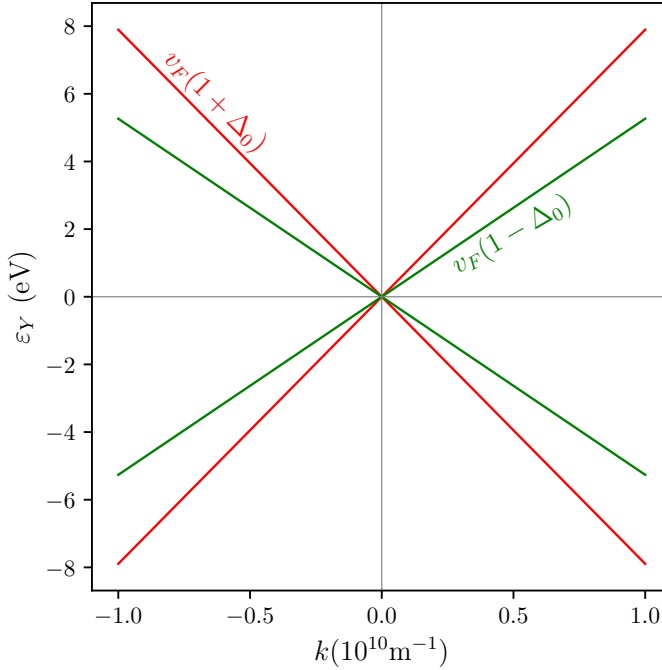


FIG. 2: (Color online) Energy dispersions $\varepsilon_Y(s, \tau | k, \Delta_0)$ for Kek-Y graphene represented by two inequivalent Dirac cones with different Fermi velocities $v_{F,1}$ and $v_{F,2}$ corresponding to $v_F(1 \pm \Delta_0)$.

subbands are often referred to as “fast” ($\tau = +1$) and “slow” ($\tau = -1$) Dirac cones, and importantly, photo-induced electronic transitions are allowed between these two.

In correspondence with energy dispersions in Eq. (7), the normalized wave functions are calculated as

$$\Psi_Y(s, \tau | \mathbf{k}, \Delta_0; \mathbf{r}) = \frac{1}{2} \begin{pmatrix} e^{-i\theta_{\mathbf{k}}} \\ s \\ s\tau \\ \tau e^{i\theta_{\mathbf{k}}} \end{pmatrix} \frac{e^{ik_x x + ik_y y}}{\sqrt{A}}, \quad (8)$$

where $\theta_{\mathbf{k}} = \tan^{-1}(k_y/k_x)$ is the angle associated with the electron wave vector \mathbf{k} with respect to the x axis. The wave function in Eq. (8) consists of two valley’s (τ_+, τ_-) sub-spinors corresponding to standard graphene eigenstates and are independent of strain applied to the system. The two valleys are related by time-reversal symmetry ($\tau_+ = -\tau_-$). Also, A is a normalization area. For which, Berry’s phase, defined as a phase difference acquired over the course of a cycle, when a system is subjected to cyclic adiabatic processes, is

$$\phi_B = -i \oint \frac{1}{4} (e^{i\theta_{\mathbf{k}}} \ s \ s\tau \ \tau e^{-i\theta_{\mathbf{k}}}) \nabla_{\mathbf{k}} \begin{pmatrix} e^{-i\theta_{\mathbf{k}}} \\ s \\ s\tau \\ \tau e^{i\theta_{\mathbf{k}}} \end{pmatrix} d\mathbf{k}. \quad (9)$$

Carrying out the derivative gives

$$\phi_B = \frac{-i}{4} \oint (e^{i\theta_{\mathbf{k}}} \ s \ s\tau \ \tau e^{-i\theta_{\mathbf{k}}}) \begin{pmatrix} -i e^{-i\theta_{\mathbf{k}}} \nabla_{\mathbf{k}} \theta_{\mathbf{k}} \\ 0 \\ 0 \\ i\tau e^{i\theta_{\mathbf{k}}} \nabla_{\mathbf{k}} \theta_{\mathbf{k}} \end{pmatrix} d\mathbf{k} \quad (10)$$

which reduces to

$$\phi_B = \frac{-i}{4}(-i + i) \oint d\theta_{\mathbf{k}} = 0. \quad (11)$$

Therefore, the Berry phase is 0 for the non-irradiated Kekulé distorted graphene as it is for the dice lattice but unlike pristine monolayer graphene for which the Berry phase has a magnitude of π . For bilayer graphene, it is 2π and that for $\alpha - T_3$ varies between 0 to π . A Berry phase of π simply applies to a pure relativistic Hamiltonian with both positive and negative energy states and that of zero represents non-relativistic Hamiltonian with only positive states and quadratic dispersion of energy with momentum. This is no longer is the case for Kek-Y distorted graphene for the zero value of Berry phase where low-energy dispersions are linear with both positive and negative states. It is associated with the equal and opposite chirality of two folded valleys at the same K-point of momentum space. This result in Eq. (11) is true for the conduction and valence bands as well as τ_+ and τ_- valleys.

III. KEK-Y DISTORTED GRAPHENE UNDER ELLIPTICALLY POLARIZED ELECTROMAGNETIC RADIATION

In the presence of an external perturbation due to an external electromagnetic wave, we can write the total Hamiltonian as $\hat{H}^T(t) = \hat{\mathcal{H}}_Y(\mathbf{k} | \Delta_0) + \hat{V}_A^{(E)}(t)$ where

$$\hat{V}_A^{(E)}(t) = \begin{pmatrix} -ev_F\sigma \cdot \mathbf{A} & \tilde{\Delta}W(t) \\ \tilde{\Delta}^*W^\dagger(t) & -ev_F\sigma \cdot \mathbf{A} \end{pmatrix}, \quad (12)$$

where $W(t) = -ev_F(A_x - iA_y)$ is expressed in terms of the vector potential $\mathbf{A}(t)$ and $\hat{V}_A^{(E)}(t)$ is periodic with period $2\pi/\Omega$. For an elliptical polarization, $\mathbf{A}^{(E)}(t)$ is given by

$$\mathbf{A}^{(E)}(t) = \begin{bmatrix} A_x^{(E)}(t) \\ A_y^{(E)}(t) \end{bmatrix} = \frac{E_0}{\Omega} \begin{bmatrix} \cos \Theta_p \cos(\Omega t) - \beta \sin \Theta_p \sin(\Omega t) \\ \sin \Theta_p \cos(\Omega t) + \beta \cos \Theta_p \sin(\Omega t) \end{bmatrix} \quad (13)$$

where E_0 is the electric-field strength, Θ_p represents the polarization angle of the optical field which is measured with respect to the normal to the surface and θ_k is the phase angle of electron wave vector which is measured with respect to the x -axis. This Hamiltonian is periodic in time and follows the time-dependent Schrödinger equation given by

$$i\hbar \frac{\partial \Psi(\mathbf{k}, \mathbf{t})}{\partial t} = \hat{H}^T(t)\Psi(\mathbf{k}, \mathbf{t}). \quad (14)$$

Based on the Floquet theorem, the solution to Eq. (14) satisfies the periodicity condition with

$$\Psi(\mathbf{k}, \mathbf{t} + \mathbf{T}) = e^{-i\mathbf{H}_{\text{eff}}\mathbf{T}/\hbar}\Psi(\mathbf{k}, \mathbf{t}), \quad (15)$$

where H_{eff} is the Floquet effective Hamiltonian, which we obtain by employing the Floquet-Magnus expansion for a high-frequency periodic field. Now, for elliptically polarized light for $\beta \neq 0$, the Floquet effective Hamiltonian for Kek-Y phase of graphene is as follows

$$H_{\text{eff}}^E(k, \Delta_0, \zeta) = \begin{pmatrix} -C(1 + \Delta_0^2) & \hbar v_f(k_x - ik_y) & \Delta_0 \hbar v_f(k_x - ik_y) & 0 \\ \hbar v_f(k_x + ik_y) & C(1 - \Delta_0^2) & 0 & \Delta_0 \hbar v_f(k_x - ik_y) \\ \Delta_0 \hbar v_f(k_x + ik_y) & 0 & -C(1 - \Delta_0^2) & \hbar v_f(k_x - ik_y) \\ 0 & \Delta_0 \hbar v_f(k_x + ik_y) & \hbar v_f(k_x + ik_y) & C(1 + \Delta_0^2) \end{pmatrix}, \quad (16)$$

where we have introduced $\tilde{\zeta} = \frac{-ev_F E_0}{\hbar \Omega^2}$ and $C = [\tilde{\zeta}^2 \beta \hbar \Omega - 2\tilde{\zeta} \beta (\hbar v_f k_x \cos \theta_p + \hbar v_f k_y \sin \theta_p)]$.

Solving the eigenvalue equation of this effective Hamiltonian, we obtained the quasiparticle energy spectrum for Kek-Y-distorted graphene under elliptically polarized electromagnetic radiation is

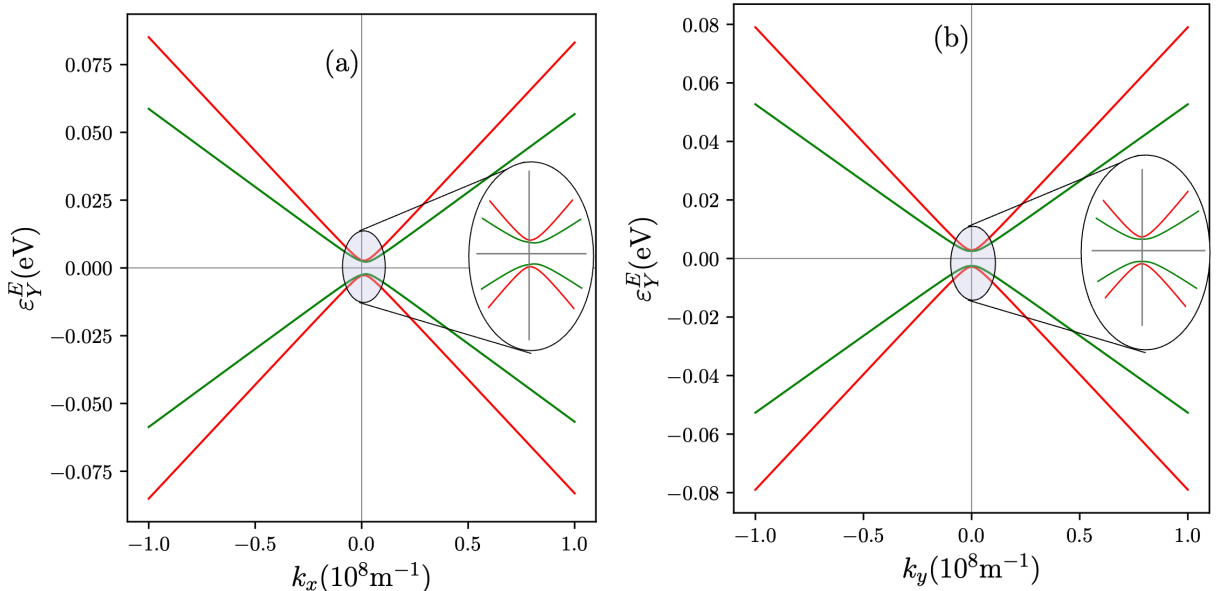


FIG. 3: (Color online) Energy dispersions $\varepsilon_Y(s, \tau | k, \Delta_0)$ for Kek-Y graphene under normal incident circularly polarized irradiation (i.e., $\theta_p = 0$, $\beta = 1$) represented by two inequivalent Dirac cones with different Fermi velocities $v_{F,1}$ and $v_{F,2}$. Plots in (a) are along k_x and plots in (b) are along k_y . The energy bands are anisotropic along two perpendicular momentum directions. In each plot, the dispersion close to the Dirac points are focused, which shows the opening of band gaps and vertical separation of the valleys. These results are for light irradiation with frequency of 100 THz, $\Delta_0 = 0.2$ and $\tilde{\zeta} = 0.1$.

$$\varepsilon_Y^E(s, \tau | k, \Delta_0, \zeta) = s \left\{ \sqrt{C^2 + \hbar^2 v_f^2 k^2} + \tau \Delta_0 \sqrt{C^2 \Delta_0^2 + \hbar^2 v_f^2 k^2} \right\}. \quad (17)$$

This type of polarized external radiation determines whether a significant gap between the cones in the valance and conduction bands is opened up at the Dirac point. The band gap between the inner cones and the gap between the outer cones are respectively given by the following equation for $\tau = \pm 1$:

$$\varepsilon_{gY}^E(\tau, \Delta_0, \zeta) = 2\hbar\Omega\tilde{\zeta}^2\beta(1 + \tau\Delta_0^2). \quad (18)$$

Additionally, the two cones are also separated by small energy $2\hbar\Omega\tilde{\zeta}^2\beta\Delta_0^2$, at $k \rightarrow 0$ in each band. The corresponding normalized wave functions are calculated as

$$\Psi_Y^E(s, \tau | \mathbf{k}, \Delta_0; \mathbf{r}) = \frac{1}{\sqrt{(b_2^2 + 1)(b_3^2 + 1)}} \begin{pmatrix} b_1(s, \tau; \mathbf{k}) e^{-i\theta_k} \\ b_2(s, \tau; \mathbf{k}) \\ b_3(s, \tau; \mathbf{k}) \\ b_4(s, \tau; \mathbf{k}) e^{i\theta_k} \end{pmatrix} \frac{e^{ik_x x + ik_y y}}{\sqrt{A}}, \quad (19)$$

where

$$\begin{aligned}
b_1(s, \tau; \mathbf{k}) &= 1 \\
b_2(s, \tau; \mathbf{k}) &= \frac{C + s\sqrt{C^2 + \hbar^2 v_f^2(k_x^2 + k_y^2)}}{\sqrt{\hbar^2 v_f^2(k_x^2 + k_y^2)}} \\
b_3(s, \tau; \mathbf{k}) &= \frac{\sqrt{\hbar^2 v_f^2(k_x^2 + k_y^2)}}{s\tau\sqrt{C^2\Delta_0^2 + \hbar^2 v_f^2(k_x^2 + k_y^2)} - C\Delta_0} \\
b_4(s, \tau; \mathbf{k}) &= \frac{C + s_1\sqrt{C^2 + \hbar^2 v_f^2(k_x^2 + k_y^2)}}{s\tau\sqrt{C^2\Delta_0^2 + \hbar^2 v_f^2(k_x^2 + k_y^2)} - C\Delta_0}
\end{aligned} \tag{20}$$

The band structure appearing in Fig. 3 is for circularly polarized light ($\beta = 1$) at normal incidence. The plotted spectrum clearly shows a small gap between the valence and conduction bands along with a vertical gap between the two cones. Notably, the bands are anisotropic along two perpendicular momentum directions. In order to include the anisotropy of the bands, the circularly polarized light at normal incidence is used in further calculation.

IV. KEK-Y VALLEY-COUPLED QUANTUM TUNNELING

For pristine graphene, the two non-equivalent Dirac K points are separated by a large momentum distance suggesting that intervalley scattering is unlikely at low energies. However, in Kek-Y graphene, the two cones are folded at same symmetry point in the Brillouin zone, making it possible for intervalley transport between the cones. The intervalley transport ensures the valley degree of freedom in graphene in the presence of strain. Since the valley precision is spatially anisotropic depending on the spacial symmetry of the material, we assume the translational symmetry to keep the transverse momentum conserve and focus our attention on the calculation of probability current for determining the transmission or reflection coefficient along the longitudinal direction. For this, we introduce a barrier $V(x) = V_0[\Theta(x) - \Theta(x - d)]$ of width d and height V_0 along the x direction of the system. The schematic illustration of electron transmission for Kek-Y distorted graphene is given in Fig. 4. In the presented figure, the outer green cone and the inner red cone represents the slow and fast cone as we explained in Sec. I. The symbols e_i , e_r , and e_t denote the incident, reflected and transmitted electron, respectively. For reference, the beam of electrons in the conduction band of the inner fast cone is incident on the potential with incident angle θ_{k+} . From the edge of the potential at $x = 0$, and $x = d$, the particle either reflects or transmits to the adjacent region. The particle from the inner cone of the incident region can appear as the particle of the outer cone in the transmission region. It means that there is finite probability for intervalley scattering. Therefore, the total probability of transmission T is the sum of the probability of transmission from the same incident cone τ^{++} and that of the other cone τ^{+-} , which we respectively called intravalley and intervalley transmission.

In general, the time-dependent Schrödinger equation for the Hamiltonian $\hat{\mathcal{H}}$ in Eq. (6) as well as the spinor-type wave function $|\Psi\rangle = [\psi_A \ \psi_B \ \psi_C \ \psi_D]^T$, can be written as $i\hbar\partial/\partial t|\Psi\rangle = \hat{\mathcal{H}}|\Psi\rangle$ from which we find that the probability density $\rho = \langle \Psi | \Psi \rangle$ satisfies

$$i\hbar\frac{\partial\rho}{\partial t} = i\hbar\frac{\partial}{\partial t}\langle \Psi | \Psi \rangle = \langle \Psi | \hat{\mathcal{H}} | \Psi \rangle - \left(\hat{\mathcal{H}} | \Psi \rangle\right)^\dagger | \Psi \rangle . \tag{21}$$

A. Tunneling and electrical conductivity without Irradiation

After substituting the Hamiltonian given in Eq. (6) into Eq. (21), we see after a lengthy calculation, that the probability current density $\mathbf{j} = \{j_x, j_y\}$ satisfies the continuity equation $\nabla \cdot \mathbf{j} + \partial\rho/\partial t = 0$, and translational invariance along the y direction further yields that j_x is conserved which is expressed as

$$j_x = v_F \{(\psi_A^* \psi_B + \psi_B^* \psi_A + \psi_C^* \psi_D + \psi_D^* \psi_C) + \Delta_0(\psi_A^* \psi_C + \psi_C^* \psi_A + \psi_B^* \psi_D + \psi_D^* \psi_B)\} . \tag{22}$$

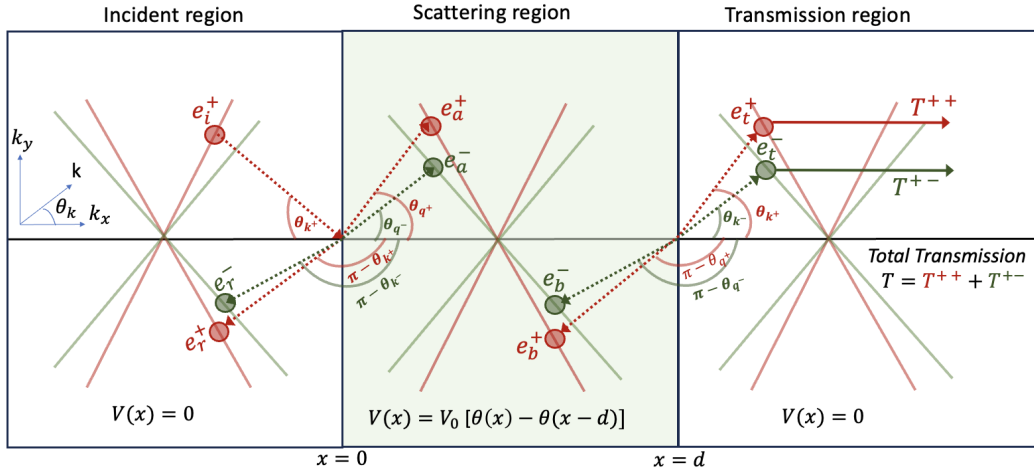


FIG. 4: (Color online) Schematics of electron transmission through potential barrier in Kek-Y graphene. The inner red and outer green cone represent the fast and slow cone or τ_+ and τ_- valley respectively. The Dirac electron e_i^+ from τ_+ valley in incident region is incident to the barrier at $x = 0$ from left with incident angle θ_{k^+} . This electron crosses the barrier of width d and height V_0 and transmit to the transmission region as a τ_+ valley electron e_t^+ with angle of transmission θ_{k^+} and probability \mathcal{T}_{++} or as a τ_- valley electron e_t^- with angle of transmission θ_{k^-} and probability \mathcal{T}_{+-} such that the total probability of transmission $\mathcal{T} = \mathcal{T}_{++} + \mathcal{T}_{+-}$. e_r^+ , e_r^- are reflected electrons through the barrier with angle of reflection $\pi - \theta_{k^+}$ and $\pi - \theta_{k^-}$ as a τ_+ valley and τ_- valley electrons respectively. e_a^+ and e_a^- are the forward moving electron at $x = 0$ in scattering region through τ_+ valley and τ_- valley making angles θ_{q^+} and θ_{q^-} respectively. Similarly, e_b^+ and e_b^- are the backward moving electron at $x = d$ in scattering region through τ_+ valley and τ_- valley making angles $\pi - \theta_{q^+}$ and $\pi - \theta_{q^-}$ respectively.

The terms $\propto \Delta_0$ clearly show the contributions to the current arising from the inter-cone coupling. The other terms are simply due to the graphene part of the Hamiltonian presented in Eq. (6).

We now consider the three regions depicted schematically in Fig. 4. Region (I) is the incident region where the particle has kinetic energy ε_k and zero potential energy. The particle on the τ_+ cone, having momentum k^+ incident from the left of the barrier of width d and constant potential height V_0 with incident angle θ_k^+ is represented by the wave function,

$$\Psi_Y^{(i)}(s, | \mathbf{k}; \mathbf{r}) = \frac{1}{2} \begin{pmatrix} e^{-i\theta_{k^+}} \\ s \\ s \\ e^{i\theta_{k^+}} \end{pmatrix} \frac{e^{i|k_x^+|x + ik_y y}}{\sqrt{\mathcal{A}}}. \quad (23)$$

From Eq. (22), the incident probability current density is calculated,

$$J_x^{(i)}(s, \mathbf{k}) = j_x^{(i)}(s, \mathbf{k}) \mathcal{A} = v_F s [1 + \Delta_0] \cos \theta_{k^+} \quad (24)$$

with $|\theta_{k^+}| \leq \pi/2$ and $k_x^+ = \frac{\varepsilon_k}{s \hbar v_F (1 + \Delta_0)} \cos(\theta_k^+)$, $k_y = \frac{\varepsilon_k}{s \hbar v_F (1 + \Delta_0)} \sin(\theta_k^+)$ and $s = \text{sign}(\varepsilon_k)$.

Region (II) is the place where the particle has interaction with the potential V_0 and is launched with initial momentum q^T corresponding to kinetic energy $|\varepsilon_k - V_0|$. The electron from the τ_+ valley in the incident region travelled through the scattering region and gets transmitted into region (III) which is referred to as the transmission region where the particle again has kinetic energy ε_k as both the transmitted and reflected electron conserve energy. When transferred to the transmission region, it either comes out to be a τ_+ valley electron or τ_- valley electron with wave functions given by

$$\Psi_Y^{(t+)}(s | \mathbf{k}; \mathbf{r}) = \frac{t_+}{2} \begin{pmatrix} e^{-i\theta_{k^+}} \\ s \\ s \\ e^{i\theta_{k^+}} \end{pmatrix} \frac{e^{i|k_x^+|x + ik_y y}}{\sqrt{\mathcal{A}}}, \quad (25)$$

and

$$\Psi_Y^{(t-)}(s | \mathbf{k}; \mathbf{r}) = \frac{t_-}{2} \begin{pmatrix} e^{-i\theta_{\mathbf{k}-}} \\ s \\ -s \\ -e^{i\theta_{\mathbf{k}-}} \end{pmatrix} \frac{e^{i|k_x^-|x+ik_y y}}{\sqrt{\mathcal{A}}} , \quad (26)$$

where $\theta_{\mathbf{k}-} = \tan^{-1}(k_y/k_x^-)$ is the angle associated with the electron wave vector $\mathbf{k}^- = \frac{\varepsilon_k}{s\hbar v_F(1-\Delta_0)}$, with respect to the x axis and t_{\pm} are the transmission coefficients which are calculated by making use of matching boundary conditions. The transmitted probability current is the sum of the current through the τ_+ valley and the τ_- valley. They are

$$J_x^{(t+)}(s, \mathbf{k}^+) = j_x^{(t+)}(s, \mathbf{k}^+) \mathcal{A} = v_F s (1 + \Delta_0) |t_+|^2 \cos(\theta_k^+) \quad (27)$$

and

$$J_x^{(t-)}(s, \mathbf{k}^-) = j_x^{(t-)}(s, \mathbf{k}^-) \mathcal{A} = v_F s (1 - \Delta_0) |t_-|^2 \cos(\theta_k^-) . \quad (28)$$

Similarly, the electrons are reflected to the incident region with the wave functions,

$$\Psi_Y^{(r+)}(s | \mathbf{k}; \mathbf{r}) = \frac{r_+}{2} \begin{pmatrix} -e^{i\theta_{\mathbf{k}+}} \\ s \\ s \\ -e^{-i\theta_{\mathbf{k}+}} \end{pmatrix} \frac{e^{-i|k_x^+|x+ik_y y}}{\sqrt{\mathcal{A}}} , \quad (29)$$

and

$$\Psi_Y^{(r-)}(s | \mathbf{k}; \mathbf{r}) = \frac{r_-}{2} \begin{pmatrix} -e^{i\theta_{\mathbf{k}-}} \\ s \\ -s \\ e^{-i\theta_{\mathbf{k}-}} \end{pmatrix} \frac{e^{-i|k_x^-|x+ik_y y}}{\sqrt{\mathcal{A}}} , \quad (30)$$

where r_{\pm} are the reflection coefficients. The reflection probability currents are given by

$$J_x^{(r+)}(s, \mathbf{k}^+) = j_x^{(r+)}(s, \mathbf{k}^+) \mathcal{A} = -v_F s (1 + \Delta_0) |r_+|^2 \cos(\theta_k^+) \quad (31)$$

and

$$J_x^{(r-)}(s, \mathbf{k}^-) = j_x^{(r-)}(s, \mathbf{k}^-) \mathcal{A} = -v_F s (1 - \Delta_0) |r_-|^2 \cos(\theta_k^-) . \quad (32)$$

In the scattering region, the electron moving forward from the potential edge $x = 0$ and moving backward from the edge $x = d$ from both $+$ and $-$ valleys has corresponding wave functions,

$$\Psi_Y^{(\gamma+)}(s' | \mathbf{q}; \mathbf{r}) = \frac{\gamma_+}{2} \begin{pmatrix} e^{-i\theta_{\mathbf{q}+}} \\ s' \\ s' \\ e^{i\theta_{\mathbf{q}+}} \end{pmatrix} \frac{e^{i|q_x^+|x+ik_y y}}{\sqrt{\mathcal{A}}} , \quad (33)$$

$$\Psi_Y^{(\gamma-)}(s' | \mathbf{q}; \mathbf{r}) = \frac{\gamma_-}{2} \begin{pmatrix} e^{-i\theta_{\mathbf{q}-}} \\ s' \\ -s' \\ -e^{i\theta_{\mathbf{q}-}} \end{pmatrix} \frac{e^{i|q_x^-|x+ik_y y}}{\sqrt{\mathcal{A}}} , \quad (34)$$

$$\Psi_Y^{(\eta_+)}(s' | \mathbf{q}; \mathbf{r}) = \frac{\eta_+}{2} \begin{pmatrix} -e^{i\theta_{\mathbf{q}^+}} \\ s' \\ s' \\ -e^{-i\theta_{\mathbf{q}^+}} \end{pmatrix} \frac{e^{-i|q_x^+|x+ik_y y}}{\sqrt{\mathcal{A}}} \quad (35)$$

and

$$\Psi_Y^{(\eta_-)}(s' | \mathbf{q}; \mathbf{r}) = \frac{\eta_-}{2} \begin{pmatrix} -e^{i\theta_{\mathbf{q}^-}} \\ s' \\ -s' \\ e^{-i\theta_{\mathbf{q}^-}} \end{pmatrix} \frac{e^{-i|q_x^-|x+ik_y y}}{\sqrt{\mathcal{A}}}, \quad (36)$$

where γ_{\pm} and η_{\pm} are the coefficients of forward moving and backward moving electrons, respectively. In this notation, q_{\pm}^{\pm} is given by $q_{\pm} \cos(\theta_q^{\pm})$ with $q_{\pm} = \frac{\varepsilon_k - V_0}{s' \hbar v_F (1 \pm \Delta_0)}$, $\theta_q^{\pm} = \sin^{-1}(k_y/q_{\pm})$ and $s' = \text{sign}(\varepsilon_k - V_0)$.

From a physical point of view, we should further introduce a set of boundary conditions for our model system. Since the relationships between the four components $\psi_A(x)$, $\psi_B(x)$, $\psi_C(x)$ and $\psi_D(x)$ of a wave function $|\Psi\rangle = (\psi_A \ \psi_B \ \psi_C \ \psi_D)^T$ have already been built into the eigenvalue equation, we use only the continuities for wave functions on both sides of the boundaries at $x = 0$ and $x = d$. The boundary condition at $x = 0$ are

$$\Psi_Y^{(i)}|_{x=0} + \Psi_Y^{(r+)}|_{x=0} + \Psi_Y^{(r-)}|_{x=0} = \Psi_Y^{(\gamma_+)}|_{x=0} + \Psi_Y^{(\gamma_-)}|_{x=0} + \Psi_Y^{(\eta_+)}|_{x=0} + \Psi_Y^{(\eta_-)}|_{x=0} \quad (37)$$

and at $x = d$

$$\Psi_Y^{(\gamma_+)}|_{x=d} + \Psi_Y^{(\gamma_-)}|_{x=d} + \Psi_Y^{(\eta_+)}|_{x=d} + \Psi_Y^{(\eta_-)}|_{x=d} = \Psi_Y^{(t_+)}|_{x=d} + \Psi_Y^{(t_-)}|_{x=d}. \quad (38)$$

From these continuity equations, we arrive at the following relations for the unknowns $(r_+, r_-, a_+, a_-, t_+, t_-)$, i.e.,

$$\begin{aligned} e^{-i\theta_{k^+}} - r_+ e^{i\theta_{k^+}} - r_- e^{i\theta_{k^-}} &= \gamma_+ e^{-i\theta_{q^+}} + \gamma_- e^{-i\theta_{q^-}} - \eta_+ e^{i\theta_{q^+}} - \eta_- e^{i\theta_{q^-}} \\ s + sr_+ + sr_- &= s' \gamma_+ + s' \gamma_- + s' \eta_+ + s' \eta_- \\ s + sr_+ - sr_- &= s' \gamma_+ - s' \gamma_- + s' \eta_+ - s' \eta_- \\ e^{i\theta_{k^+}} - r_+ e^{-i\theta_{k^+}} + r_- e^{-i\theta_{k^-}} &= \gamma_+ e^{i\theta_{q^+}} - \gamma_- e^{i\theta_{q^-}} - \eta_+ e^{-i\theta_{q^+}} + \eta_- e^{-i\theta_{q^-}} \\ \gamma_+ e^{-i\theta_{q^+} + iq_x^+ d} + \gamma_- e^{-i\theta_{q^-} - iq_x^- d} - \eta_+ e^{i\theta_{q^+} - iq_x^+ d} - \eta_- e^{i\theta_{q^-} - iq_x^- d} &= t_+ e^{-i\theta_{k^+} + ik_x^+ d} + t_- e^{-i\theta_{k^-} + ik_x^- d} \\ \gamma_+ s' e^{iq_x^+ d} + \gamma_- s' e^{iq_x^- d} + \eta_+ s' e^{-iq_x^+ d} + \eta_- s' e^{-iq_x^- d} &= t_+ s e^{ik_x^+ d} + t_- s e^{ik_x^- d} \\ \gamma_+ s' e^{iq_x^+ d} - \gamma_- s' e^{iq_x^- d} + \eta_+ s' e^{-iq_x^+ d} - \eta_- s' e^{-iq_x^- d} &= t_+ s e^{ik_x^+ d} - t_- s e^{ik_x^- d} \\ \gamma_+ e^{i\theta_{q^+} + iq_x^+ d} - \gamma_- e^{i\theta_{q^-} + iq_x^- d} - \eta_+ e^{-i\theta_{q^+} - iq_x^+ d} + \eta_- e^{-i\theta_{q^-} - iq_x^- d} &= t_+ e^{i\theta_{k^+} + ik_x^+ d} - t_- e^{i\theta_{k^-} + ik_x^- d}. \end{aligned} \quad (39)$$

Since the analytical solutions of these equations are very lengthy and time consuming we employed the numerical method explained in appendix A. Using these results for the t_+, t_-, r_+ and r_- , one can calculate the probability of transmission and reflection through each valley as follows,

$$\mathcal{T}_{++} = \frac{|J_x^{(t_+)}|}{|J_x^{(i)}|} = |t_+|^2, \quad (40)$$

$$\mathcal{T}_{+-} = \frac{|J_x^{(t_-)}|}{|J_x^{(i)}|} = |t_-|^2 \frac{(1 - \Delta_0) \cos \theta_{k^-}}{(1 + \Delta_0) \cos \theta_{k^+}}, \quad (41)$$

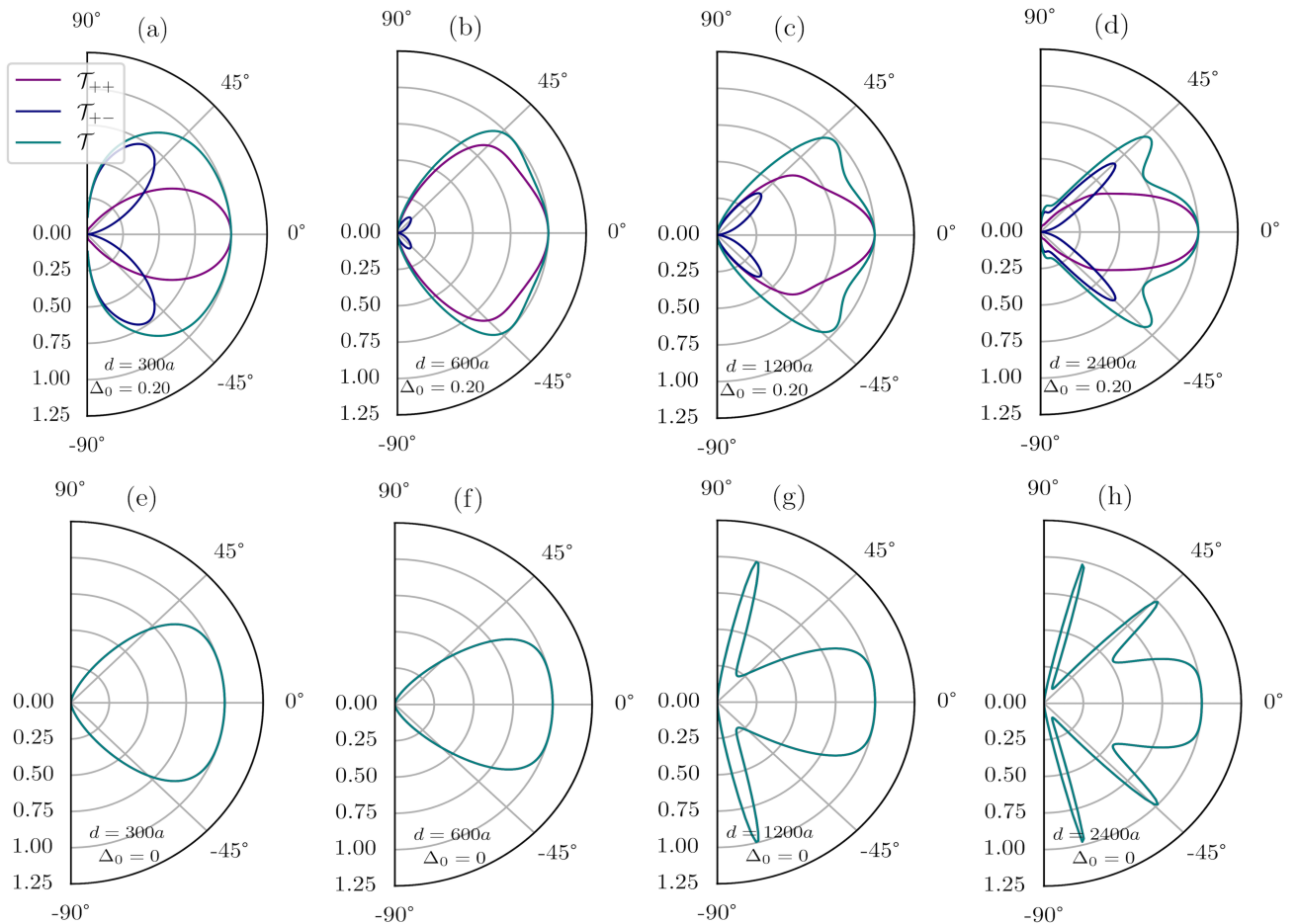


FIG. 5: (Color online) Valley resolved angular transmission of monolayer Kek-Y graphene through a potential barrier of uniform height. Polar plots (a), (b), (c) and (d) in the upper panel are for barrier width d equal $300a$, $600a$, $1200a$ and $2400a$, respectively, with Kekulé parameter $\Delta_0 = 0.2$. Plots (e), (f), (g) and (h) in the lower panel are for undistorted graphene with $\Delta_0 = 0$ with corresponding barrier width, in the absence of irradiation. Here, $a = 2.46\text{\AA}$ is the lattice constant of graphene. The energy of the incident particle is $\varepsilon_Y = 0.028\text{eV}$ and the potential height is $V_0 = 3\varepsilon_Y$. The notation \mathcal{T}_{++} represents the intravalley transmission from the τ_+ valley to τ_+ valley while \mathcal{T}_{+-} represents the intervalley transmission from the τ_+ valley to the τ_- valley. The total transmission is $\mathcal{T} = \mathcal{T}_{++} + \mathcal{T}_{+-}$. For undistorted graphene in the lower panel, the transmission is through only one valley. Klein tunneling at normal incidence is preserved in both distorted and undistorted graphene.

$$\mathcal{R}_{++} = \frac{|J_x^{(r_+)}|}{|J_x^{(i)}|} = |r_+|^2 \quad (42)$$

$$\mathcal{R}_{+-} = \frac{|J_x^{(r_-)}|}{|J_x^{(i)}|} = |r_-|^2 \frac{(1 - \Delta_0) \cos \theta_{k-}}{(1 + \Delta_0) \cos \theta_{k+}} \quad (43)$$

so that the total transmission $\mathcal{T} = \mathcal{T}_{++} + \mathcal{T}_{+-}$ and the total reflection $\mathcal{R} = \mathcal{R}_{++} + \mathcal{R}_{+-}$.

Let us now analyze some specific situations we encountered.

(i) When $\Delta_0 \neq 0$ and 1, the two valleys at the edge of the hexagonal Brillouin zone in monolayer gapless graphene come to the center of the Brillouin zone and get folded at the Γ point. This means that for Kek-Y distorted graphene, the distance between valleys is zero in reciprocal space since one Dirac cone gets buried inside the other and hence even with the same lattice scale as pristine graphene, the potential can vary sharply causing the particle to scatter from one valley to another. Therefore, the electron from one valley has finite probability to appear as an another valley electron when it passes through the potential barrier which we refer to as intervalley transmission. It is such that the total probability of transmission is the sum of the probability as an one valley as well as another valley electron. This type of valley resolved scattering opens a new topological platform for use as a valley degree of freedom. However, in pristine graphene on the lattice scale, the intervalley scattering is not possible as the separation between two valleys in reciprocal space is equal to the reciprocal of the lattice constant. Under this condition, the potential varies smoothly and valleys are independent. Hence, intervalley scattering is forbidden. The numerical results for the transmission probability at different angles and chosen width of the barrier for Kek-Y distorted graphene at $\Delta_0 = 0.2$ are presented in Fig. 5. In the displayed figure, the transmission probability is 1 around normal incidence regardless of width of the barrier for potential three times higher than that of incident energy ε_Y . This perfect transmission even for the barrier higher than that of the energy of incident beam is known as Klein tunneling⁴⁵. However, Allain in Ref. [46], has argued that perfect transmission at normal incidence is not a genuine Klein tunnelling as it does not incorporate any classically forbidden region and neither even any evanescent or quickly decaying waves are present. It is due to the presence of the valance band state and conduction band state at the boundary of the potential where they matched, and also due to the pseudospin conservation or due to the pseudo-spin flip at two sublattices where the waves are continuous to move forward. This is discussed as the chiral behavior of graphene that prevents backscattering and gives perfect transmission for the normally incident beam.

As we see from Fig.5, the transmission does not only depend on the angle of incidence, it also is a function of the incident particle energy, height and width of the barrier and also the Kekulé parameter Δ_0 . For example, the region for perfect transmission for $d = 300a$ is about $\theta_{k+} \leq \pi/6$ and is reduced when the barrier width is increased. It is true only for normal incidence for a potential step with infinite barrier width. It is also seen that the intervalley scattering does not exist at around normal incidence and there is perfect reflection at $\theta_{k+} = \pi/2$.

- (ii) When $\Delta_0 = 0$, the energy dispersion comes out to be that of pristine graphene. In this case, the numerical results for the transmission and reflection probability reproduce those for gapless graphene in Ref. [47]. Figure 5 shows that in the lower panel for Δ_0 equal to zero, the transmission is only due to intravalley transmission. For gapless monolayer graphene for normal incidence i.e., $\theta_{k+} = 0$, $|\mathcal{T}| = 1$ irrespective of the kinetic energy of the incident beam. For wider potential barrier, perfect transmission is observed at some points besides normal incidence or it oscillates between 1 and 0 similar to the sine and cosine functions which is due to resonance scattering. Such resonance tunneling is suppressed when the intervalley transmission is taken into account for $\Delta_0 \neq 0$. In contrast to perfect transmission through monolayer graphene, bilayer graphene shows perfect reflection at normal incidence⁴⁵. Although both the negative energy states and positive energy states are present at the boundary, chirality does not allow the transmitted wave to travel in the forward direction. Since the Berry phase of bilayer graphene is 2π instead of π the pseudospin is not conserved between two sublattices, creating the wave quickly, vanishes in the potential region, enhancing the backscattering to the incident region.
- (iii) When $\Delta_0 = 1$, the outer valley for $\tau = -1$, becomes dispersionless. At around normal incidence, all the electrons from outer flat band couples to the inner dispersive band and hence crosses the junction giving rise to super-Klein tunneling⁴⁸. This extreme condition has not been considered for calculation which is beyond the scope of this manuscript.

We should mention that in the above calculation only the longitudinal momentum k_x is changes, keeping the transverse momentum k_y conserved assuming translational symmetry along the y direction. Therefore the observed transmission is for the longitudinal transmission. Besides the translational symmetry, the material also preserves inversion symmetry. We note that as we are interested in seeing Klein tunneling, we have considered the potential much higher than that of the energy of incident particle which is equal to 0.028 eV in our numerical results.

1. Electrical conductivity using Landauer-Buttiker formalism

In quantum mechanics, the electrical conductance can be calculated by using the Landauer formula for ballistic transport⁴⁹ at 0 K, which necessitates a calculation of the transmission probability. It is given by

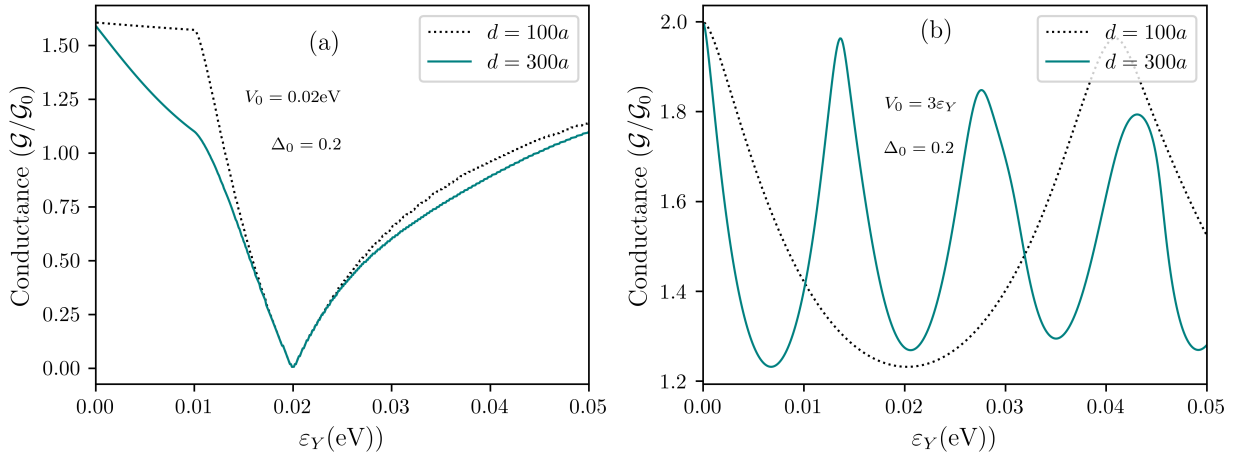


FIG. 6: (Color online) Quantum conductance of ballistic transport for Kek-Y distorted graphene across a potential barrier of width d . The coefficient of conductance $\mathcal{G}/\mathcal{G}_0$ is plotted as a function of the kinetic energy of an incident electron for chosen potential height $V_0 = 0.02\text{eV}$ in (a) and for barrier height equal to 3 times the incident energy in (b).

$$\mathcal{G} = \frac{2e^2}{h} \mathcal{T} \quad (44)$$

where \mathcal{T} is the electron transmission probability through all possible modes. For specific valley and spin orientation, it can be expressed as

$$\mathcal{G} = \mathcal{G}_0 \int_{-\pi/2}^{\pi/2} d\theta_k \cos \theta_k \mathcal{T}(\theta_k) \quad (45)$$

where $\mathcal{G}_0 = \frac{2e^2}{h}$ is the conductance quantum and $\mathcal{T}(\theta_k) = \sum_{\tau, \tau'} \mathcal{T}_{\tau, \tau'}(\theta_k)$, for $\tau, \tau' = \pm$.

In Fig. (6), we present numerical results for the electrical conductance through a potential barrier in Kek-Y graphene, in the absence of irradiation as a function of kinetic energy for an electron in the presence of a barrier of height larger than the kinetic energy of the incident electron. As the energy is increased, the conductance exhibits periodic oscillations and we observe a dip in the conductance when the electron energy is close to the barrier height. This is due to the reduction in the transmission probability in that regime.

B. Effect on tunneling due to circularly Polarized Irradiation

We now focus our attention on the effect due to irradiation on transmission and reflection of particles across a potential barrier. With the Hamiltonian in Eq. (16), the energy eigenvalues in Eq. (17) and eigenvectors in Eq. (19), we obtain the probability current density j_x along the longitudinal direction as

$$\begin{aligned} j_x = & v_f [(\psi_A^* \psi_B + \psi_B^* \psi_A + \psi_C^* \psi_D + \psi_D^* \psi_C) + \Delta_0 (\psi_A^* \psi_C + \psi_C^* \psi_A + \psi_B^* \psi_D + \psi_D^* \psi_B)] \\ & + 2v_f \tilde{\zeta} (1 + \Delta_0^2) (\psi_A^* \psi_A - \psi_D^* \psi_D) + 2v_f \tilde{\zeta} (1 - \Delta_0^2) (\psi_C^* \psi_C - \psi_B^* \psi_B) \end{aligned} \quad (46)$$

Additionally, in the presence of irradiation, we consider an electron from the τ_+ valley, which yields the incident current

$$J_x^{(i)} = 2v_f \left[\left(\frac{b_s(\theta_{k+})}{1 + b_s^2(\theta_{k+})} + \Delta_0 \frac{b_\tau(\theta_{k+})}{1 + b_\tau^2(\theta_{k+})} \right) \cos \theta_{k+} + \tilde{\zeta} \left(\frac{1 - b_s^2(\theta_{k+})}{1 + b_s^2(\theta_{k+})} + \Delta_0^2 \frac{1 - b_\tau^2(\theta_{k+})}{1 + b_\tau^2(\theta_{k+})} \right) \right] \quad (47)$$

with the corresponding incident wave function

$$\Psi_Y^{E(i)}(\mathbf{k}; \mathbf{r}) = \frac{1}{\sqrt{(1 + b_s^2(\theta_{k^+}))(1 + b_+^2(\theta_{k^+}))}} \begin{pmatrix} e^{-i\theta_{k^+}} \\ b_s(\theta_{k^+}) \\ b_+(\theta_{k^+}) \\ b_s(\theta_{k^+})b_+(\theta_{k^+})e^{i\theta_{k^+}} \end{pmatrix} \frac{e^{ik_y y + i|k_x^+|x}}{\sqrt{A}}. \quad (48)$$

Similarly, the transmitted and reflected current with transmitted and reflected wave functions are presented in the Appendix B. Here, the parameters are defined as follows

$$k_\tau = \frac{\varepsilon_Y^E}{s\hbar v_F[(1 + \tau\Delta_0) + 2\tilde{\zeta}^2 \cos^2 \theta_{k^\tau}(1 + \tau\Delta_0^3)]} \quad (49)$$

with

$$\varepsilon_Y^E = s \left\{ \sqrt{C^2 + \hbar^2 v_f^2 k^2} + \tau\Delta_0 \sqrt{C^2 \Delta_0^2 + \hbar^2 v_f^2 k^2} \right\} \quad (50)$$

and $C = \tilde{\zeta}^2 \hbar v - 2\tilde{\zeta} \hbar v_F k \cos \theta_k$. We assume that, $\zeta \ll \hbar\Omega$, $\zeta \ll \hbar v_F k$ and perform a Taylor expansion from which we obtain $C = -2\tilde{\zeta} \hbar v_F k \cos \theta_k$ and $\varepsilon_Y^E = s\hbar v_F[(1 + \tau\Delta_0) + 2\tilde{\zeta}^2 \cos^2 \theta_k(1 + \tau\Delta_0^3)]$, where $\tilde{\zeta} = \zeta/\hbar\Omega$ so that we neglected the higher order terms of $\tilde{\zeta}$. From the expression for ε_Y^E and k_τ , we can calculate $k_x^\tau = k_\tau \cos \theta_{k^\tau}$ and $k_y = k_\tau \sin \theta_{k^\tau}$, ($\tau = +$ for an incident particle from the τ_+ valley). Similarly, $b_s(\theta_{k^\tau}) = s(1 + 2\tilde{\zeta}^2 \cos^2 \theta_{k^\tau} - 2s\tilde{\zeta} \cos \theta_{k^\tau})$ and $b_\tau(\theta_{k^\tau}) = s\tau/(1 + 2\Delta_0^2 \tilde{\zeta}^2 \cos^2 \theta_{k^\tau} + 2s\tau\Delta_0 \tilde{\zeta} \cos \theta_{k^\tau})$, where $s = \text{sign}(\varepsilon_Y^E)$.

The incident, reflected and transmitted waves are from the (I) and (III) regions in the schematic in Fig. 4. In the scattering region (II), the forward moving and backward moving waves with their corresponding coefficients are given in the Appendix B. Making use of the boundary conditions at $x = 0$ and $x = d$, we solve for \tilde{r}_+ , \tilde{r}_- , \tilde{t}_+ , \tilde{t}_- .

Now, the probability of the transmission and reflection through each valley in the presence of irradiation in terms of these coefficients can be expressed as follows,

$$\tilde{\mathcal{T}}_{++} = \frac{|J_x^{(\tilde{t}_+)}|}{|J_x^{(i)}|} = |\tilde{t}_+|^2, \quad (51)$$

$$\tilde{\mathcal{T}}_{+-} = \frac{|J_x^{(\tilde{t}_-)}|}{|J_x^{(i)}|} = |\tilde{t}_-|^2 \alpha \quad (52)$$

$$\tilde{\mathcal{R}}_{++} = \frac{|J_x^{(\tilde{r}_+)}|}{|J_x^{(i)}|} = |\tilde{r}_+|^2 \lambda \quad (53)$$

and

$$\tilde{\mathcal{R}}_{+-} = \frac{|J_x^{(\tilde{r}_-)}|}{|J_x^{(i)}|} = |\tilde{r}_-|^2 \kappa \quad (54)$$

so that the total transmission $\tilde{\mathcal{T}} = \tilde{\mathcal{T}}_{++} + \tilde{\mathcal{T}}_{+-}$ as well as the total reflection $\tilde{\mathcal{R}} = \tilde{\mathcal{R}}_{++} + \tilde{\mathcal{R}}_{+-}$. Here, α , λ and κ are given in the Appendix B.

The application of circularly polarized irradiation on Kek–Y graphene opens up a small gap between the valence and conduction bands near the Dirac point. It also produces a small energy difference near the minima of the two

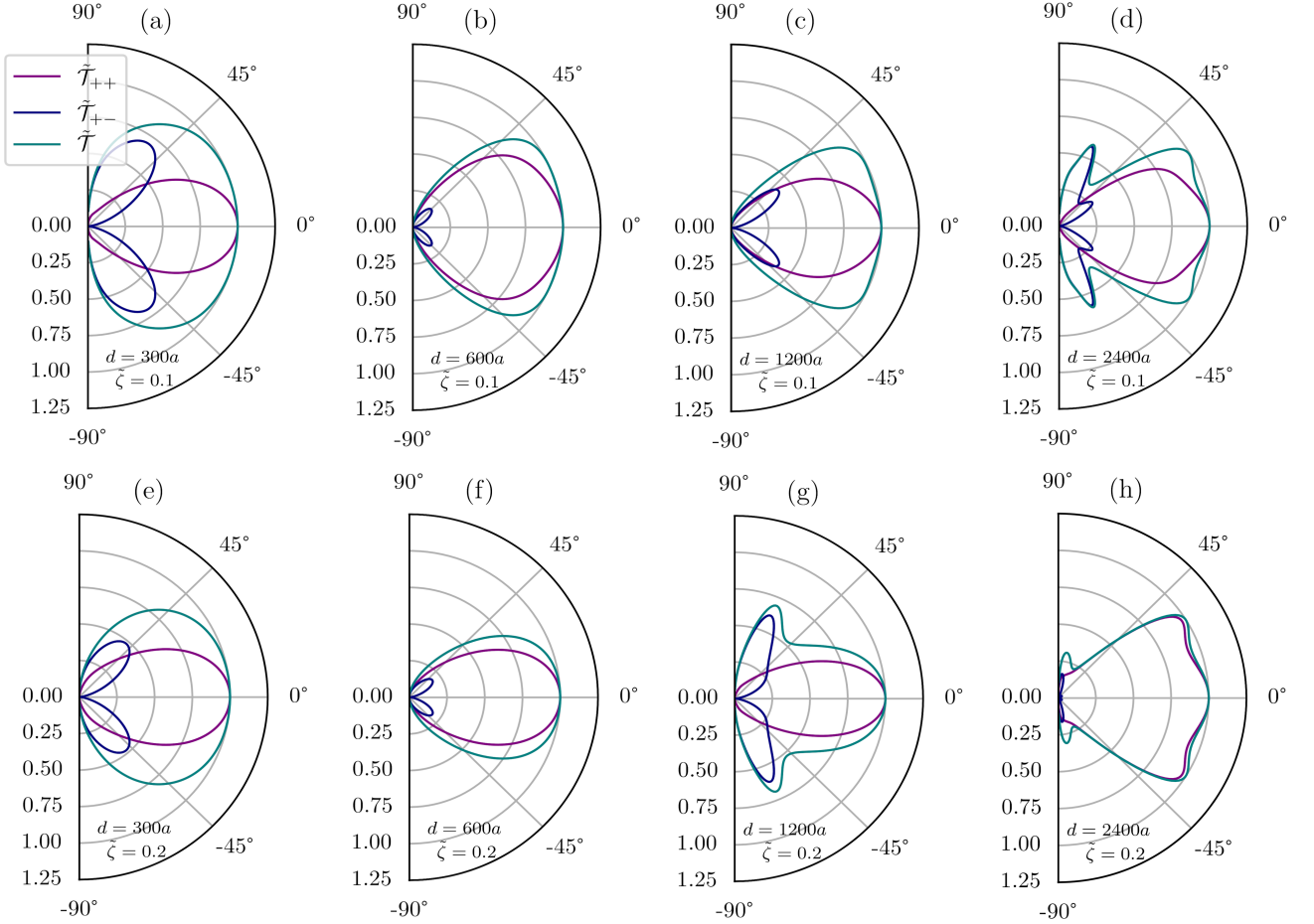


FIG. 7: (Color online) Valley resolved angular transmission of monolayer Kek-Y graphene across a potential barrier of uniform height in the presence of circularly polarized light. Plots (a), (b), (c) and (d) in the upper panel are for barrier width d equal to $300a$, $600a$, $1200a$ and $2400a$, respectively, for radiation parameter $\tilde{\zeta} = 0.1$. Plots (e), (f), (g) and (h) in the lower panel are for $\tilde{\zeta} = 0.2$ for corresponding barrier width. Here, $a = 2.46\text{\AA}$ is the lattice constant of graphene. The energy of the incident particle is $\varepsilon_Y = 0.028$ eV and the height of the potential is chosen as $V_0 = 3\varepsilon_Y$. We have chosen the Kekulé parameter $\Delta_0 = 0.2$. In our notation, $\tilde{\mathcal{T}}_{++}$ represents intravalley transmission from the τ_+ valley to the τ_+ valley while $\tilde{\mathcal{T}}_{+-}$ representing intervalley transmission from the τ_+ valley to the τ_- valley. The total transmission $\tilde{\mathcal{T}} = \tilde{\mathcal{T}}_{++} + \tilde{\mathcal{T}}_{+-}$. Klein tunneling at normal incidence is preserved even in the presence of high-frequency radiation.

folded valleys but it does not affect the chirality, the same as in the absence of irradiation. The bands become anisotropic along the longitudinal momentum direction for $\theta_p = 0$ and hence the inversion symmetry is broken. In a recent paper, Wang¹⁶ has shown that addition of site energy modification in Y-shaped Kekulé pattern breaks the inversion symmetry and which also enhances Klein tunneling. Our numerical results showing the effect due to circularly polarized irradiation on valley resolved transmission of an electron across the potential barrier in Kek-Y graphene are presented in Fig. 7. We note that the irradiation is not so strong since we have considered the illumination energy to be about 0.1 eV. All other parameters employed to calculate the results are revealed in the figure caption. The results shown in the upper panel of the figure were obtained in the presence of radiation with parameter $\tilde{\zeta} = 0.1$. This means that the frequency of the impinging electromagnetic wave is about 100 THz and the intensity of the field is about 3000 V/m. In this case, the transmission is not significantly affected for the smaller barrier width. However, as the barrier width is increased, the transmission is reduced for incident angle other than normal incidence. Perfect transmission for normal incidence is still preserved even in the presence of an EM field. Although the inversion symmetry is broken due to irradiation it did not enhance the transmission. The reduction of the transmission probability seems to be a consequence of intervalley scattering. When the eigenstates are dressed, they are less likely to change their velocity in the scattering region. The range of the angle of incidence for perfect transmission is further reduced when the

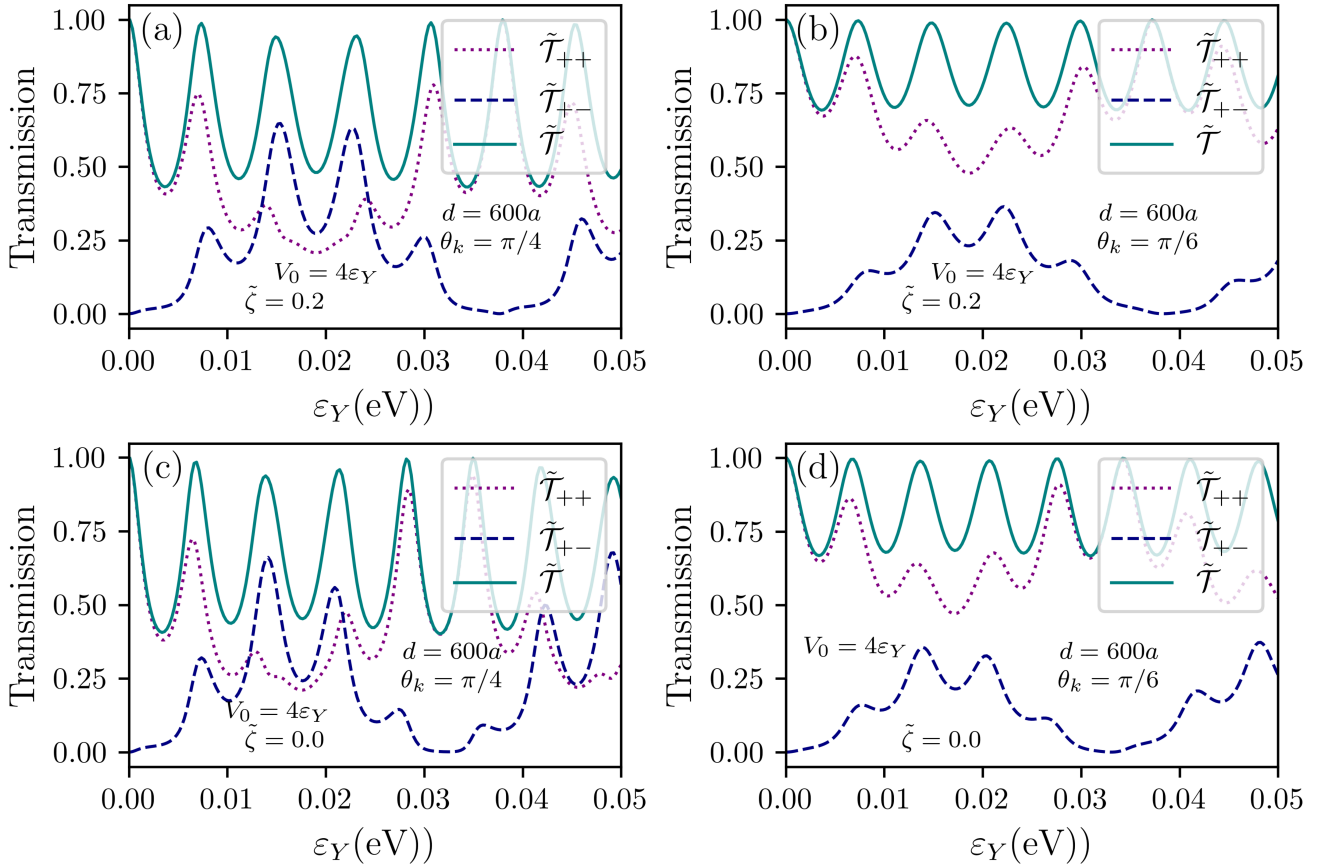


FIG. 8: (Color online) Valley resolved transmission of monolayer Kek-Y graphene through a potential barrier of constant height as a function of kinetic energy of the incident particle. Plots (a) and (b) in the upper panel are in the presence of circularly polarized light with irradiation parameter $\tilde{\zeta} = 0.2$ for incident angles $\pi/4$ and $\pi/6$, respectively, whereas plots (c) and (d) in the lower panel are for the same angle of incidence but in the absence of irradiation. The chosen height of the potential barrier is $V_0 = 4\epsilon_Y$ and the width is $d = 600a$. Here, $a = 2.46\text{\AA}$ is the lattice constant of graphene. We have chosen the Kekulé parameter $\Delta_0 = 0.2$. The symbol \tilde{T}_{++} represents the intravalley transmission from the τ_+ valley to the τ_+ valley while \tilde{T}_{+-} denotes intervalley transmission from the τ_+ valley to the τ_- valley. The total transmission $\tilde{T} = \tilde{T}_{++} + \tilde{T}_{+-}$.

radiation intensity is made stronger. Which is seen in the plots in the lower panel of Fig. 7 which were computed for $\zeta = 0.2$. It suggests that illuminating the material with electromagnetic irradiation does not enhance the conditions for Klein tunneling in Kek-Y graphene although irradiation has other significant benefits in 2D materials.

Since the gap opening is due to irradiation, one should know what would be the effect on the transmission when we change the energy of the incident particle around the gap. This is one of the interesting events we would like to address. For this, we have shown the transmission as a function of incident energy in Fig. 8 for two chosen incident angles. For the given parameters in the figure, a band gap of approximately 5.6 meV is opened and the gap between two valleys is around 2.5 meV. In the plots (a) and (b) of Fig. 8, the radiation parameter is chosen as 0.2 and the potential is four times that of the incident energy. The total transmission is oscillatory between 0.5 and 1.0 for an incident angle $\pi/4$ and between 0.75 and 1.0 for incident angle $\pi/6$ as a function of energy. When the energy of an incident particle is very small in the vicinity of the gap, and the potential is very high, the transmission is totally due to intravalley scattering. However, when the incident energy is increased and becomes larger than the gap, the intervalley scattering becomes dominant. For comparison, the results in the absence of irradiation are plotted in (c) and (d) in the lower panel. All these results show that the transmission depends on all the factors such as the energy of the incident particle, the potential width and height, irradiation parameter and angle of incidence. If we carefully choose these quantities for an experiment, we can tune the Klein tunneling and hence the electrical conductivity of the material which we will discuss in another section.

V. EXCITON-ASSISTED TUNNELING IN GAPPED KEK-Y GRAPHENE

The quantum tunneling of a bound electron-hole pair across a potential barrier is governed by its mass in the center of mass frame of reference as well as the binding energy of the pair. Since the binding energy of the exciton is quite large and due to its finite effective mass, the tunneling of excitons through an atomic scale barrier is significant in a 2D material. Here, we use the general formalism presented by Kavka³⁸ for quantum mechanical tunneling and reflection of an exciton in a single bound state incident upon a potential barrier to demonstrate the multichannel transport of excitons. We will also present the transmission and reflection probability dependent on the irradiation parameter which plays a role in opening an energy bandgap for the system.

Let us consider an electron of mass m_e , with position coordinate x_e , in the conduction band and a hole of mass m_h , with coordinate x_h , in the valance band of Kek-Y graphene under circularly polarized light. These two particles are bound by the attractive Coulomb potential $V(r) = -e^2/\epsilon_s|x|$ where $\epsilon_s \equiv 4\pi\epsilon_0\epsilon_b$ with ϵ_b denoting the background dielectric constant. The electron experiences an external potential barrier $V_e(x_e)$ and the hole is subjected to $V_h(x_h)$. The Hamiltonian for this system is given by,

$$\mathbf{H} = -\frac{\hbar^2}{2M} \frac{\partial^2}{\partial X^2} - \frac{\hbar^2}{2\mu} \frac{\partial^2}{\partial x^2} - i\hbar \frac{3v_{Fx}}{2} \frac{\partial}{\partial X} + V_e(X - \frac{\mu}{m_e}x) + V_h(X + \frac{\mu}{m_h}x) - \frac{e^2}{\epsilon_s|x|} , \quad (55)$$

where $M = m_e + m_h$ and $\mu = m_e m_h / M$ are center of mass and relative mass of the electron-hole pair and $X = \frac{m_e x_e + m_h x_h}{m_e + m_h}$ and $x = x_e - x_h$ are their corresponding coordinates. The third term proportional to v_{Fx} is due to the linear term in the Taylor expansion of the energy eigenvalue in Eq. (17). Also, $v_{Fx} = 2v_F\tilde{\zeta}(1 + \tau\Delta_0^2)$ is the group velocity and $m_{e,h} = \frac{\tilde{\zeta}^2\hbar\Omega}{v_F^2(1+\tau)}$ is the effective mass of the electron or hole. Since for the outer valley, $\tau = -1$, the mass diverges. This signifies that the zero curvature of the electron subband near the Dirac point for dressed states is due to circularly polarized irradiation. The electron or hole in this valley does not contribute to the transmission or electrical conductivity. Therefore, we will confine our numerical calculations for electron or hole tunneling from the inner valley with $\tau = +1$. We solved for the eigenvalue and eigenfunction for the exciton by using the method of separation of variables. The solutions of the one dimensional hydrogen atom problem were discussed in our paper.⁵⁰ These are ,

$$E_p = -\frac{\mu(e^2/\epsilon_s)^2}{2\hbar^2(p-1/2)^2} = -\frac{\hbar^2}{2\mu a_e^2(p-1/2)^2} \quad (56)$$

and

$$\phi_p(z) = N_p z e^{-|z|/2} L_{p+1}^1(|z|) \quad (57)$$

where $p = 0, 1, 2, \dots$, $z = 2x/[(p+1)a_e]$, $N_p = 1/[2(p+2)]$ is a normalization constant and $a_e = \hbar^2\epsilon_s/e^2\mu$ is the exciton Bohr radius. With these values for the eigenfunctions and eigenvalues, the Schrödinger-Dirac equation becomes

$$\mathbf{H}\psi(x, X) = \varepsilon_Y\psi(x, X) \quad (58)$$

such that $\psi(x, X) = \phi_p(x)\xi_p(X)$ and $\varepsilon_Y = E_p + E'_p$.

$$\left(\frac{d^2}{dX^2} + i\hbar \frac{6m_{e,h}v_{Fx}}{\hbar^2} \frac{d}{dX} + K_m^2 \right) \xi_m(X) + \sum_p Z_{mp}(X) \xi_p(X) = 0 , \quad (59)$$

where, $Z_{mp}(X) = \frac{4m_{e,h}}{\hbar^2} \int_{-\infty}^{\infty} dx \phi_m^*(x)\phi_p(x)[V_e(X - x/2) + V_h(X + x/2)]$ is the effective potential for the center of mass and $K_m^2 = \frac{4m_{e,h}}{\hbar^2}(\varepsilon_Y - E_m)$ is the center of mass wave number for an exciton in state m . The effective potential $Z_{mp}(X)$ can be thought of as the potential barrier that the center of mass encounters while incident in the state p and reflected or transmitted in the state m . Equation (59) can be rewritten in the form as

$$\left(\frac{d^2}{dX^2} + K_m'^2 \right) \xi'_m(X) + \sum_p Z_{mp}(X) \xi'_p(X) = 0 , \quad (60)$$

where $K_m'^2 = K_m^2 - \left(\frac{3m_{e,h}v_Fx}{\hbar}\right)^2$, $\xi_m(X) = e^{-i\frac{3m_{e,h}v_Fx}{\hbar}X}\xi'_m(X)$ and $\xi_p(X) = e^{i\frac{3m_{e,h}v_Fx}{\hbar}X}\xi'_p(X)$.

If a plane wave from left of the barrier is incident in the n^{th} state of the exciton, then we can find the formal solution of Eq. (60) is

$$\xi'_{mn}(X) = e^{iK'_m X} \delta_{mn} + \frac{1}{2iK'_m} \sum_{p=0}^{\infty} \int_{-\infty}^{\infty} e^{iK'_m |X-X'|} Z_{mp}(X') \xi'_{pn}(X') dX'. \quad (61)$$

Since $\xi_m(X) = e^{-i\frac{3m_{e,h}v_Fx}{\hbar}X}\xi'_m(X)$ and $\xi_p(X) = e^{i\frac{3m_{e,h}v_Fx}{\hbar}X}\xi'_p(X)$, the solution of Eq. (59) which is employed to calculate the reflection and transmission coefficient and is given by

$$\xi_{mn}(X) = e^{i\left(K'_m - \frac{3m_{e,h}v_Fx}{\hbar}\right)X} \delta_{mn} + \frac{1}{2iK'_m} \sum_{p=0}^{\infty} \int_{-\infty}^{\infty} dX' e^{i\left(K'_m - \frac{3m_{e,h}v_Fx}{\hbar}\right)|X-X'|} Z_{mp}(X') \xi_{pn}(X'), \quad (62)$$

which we use to define the reflection and transmission amplitudes, i.e.,

$$R_{mn} = \frac{1}{2iK'_m} \sum_{p=0}^{\infty} \int_{-\infty}^{\infty} dX' e^{i\left(K'_m - \frac{3m_{e,h}v_Fx}{\hbar}\right)X'} Z_{mp}(X') \xi_{pn}(X') \quad (63)$$

and

$$T_{mn} = \delta_{mn} + \frac{1}{2iK'_m} \sum_{p=0}^{\infty} \int_{-\infty}^{\infty} dX' e^{-i\left(K'_m - \frac{3m_{e,h}v_Fx}{\hbar}\right)X'} Z_{mp}(X') \xi_{pn}(X'). \quad (64)$$

Next, we followed the procedure developed by Razavy⁵¹, and we obtained coupled differential equations for the variable reflection and transmission coefficients as,

$$\begin{aligned} \frac{dR_{mn}(y)}{dy} &= - \sum_{j=0}^{\infty} \frac{1}{2iK'_j} \left\{ e^{i\left(K'_j - \frac{3m_{e,h}v_Fx}{\hbar}\right)y} \delta_{mj} + R_{mj}(y) e^{-i\left(K'_j - \frac{3m_{e,h}v_Fx}{\hbar}\right)y} \right\} \\ &\times \sum_{p=0}^{\infty} Z_{jp}(y) \left\{ e^{i\left(K'_p - \frac{3m_{e,h}v_Fx}{\hbar}\right)y} \delta_{pn} + R_{pn}(y) e^{-i\left(K'_p - \frac{3m_{e,h}v_Fx}{\hbar}\right)y} \right\} \end{aligned} \quad (65)$$

and

$$\begin{aligned} \frac{dT_{mn}(y)}{dy} &= - \sum_{j=0}^{\infty} \frac{1}{2iK'_j} \left\{ e^{i\left(K'_j - \frac{3m_{e,h}v_Fx}{\hbar}\right)y} T_{mj}(y) \right\} \\ &\times \sum_{p=0}^{\infty} Z_{jp}(y) \left\{ e^{i\left(K'_p - \frac{3m_{e,h}v_Fx}{\hbar}\right)y} \delta_{pn} + R_{pn}(y) e^{-i\left(K'_p - \frac{3m_{e,h}v_Fx}{\hbar}\right)y} \right\} \end{aligned} \quad (66)$$

with the boundary conditions

$$\begin{aligned} R_{mn}(y \rightarrow \infty) &= 0 & R_{mn}(y \rightarrow -\infty) &= R_{mn} \\ T_{mn}(y \rightarrow \infty) &= \delta_{mn} & T_{mn}(y \rightarrow -\infty) &= T_{mn}. \end{aligned} \quad (67)$$

By solving these equations for R_{mn} and T_{mn} we will calculate the total probability of transmission and reflection of an exciton incident on the state n , which is given by the expressions,

$$\begin{aligned} R &= \sum_m \frac{K'_m}{K'_n} |R_{mn}|^2 \\ T &= \sum_m \frac{K'_m}{K'_n} |T_{mn}|^2. \end{aligned} \quad (68)$$

In this notation, $K'_m = \left\{ \frac{4m_{e,h}(\varepsilon_Y - E_m)}{\hbar^2} - \left(\frac{3m_{e,h}v_{Fx}}{\hbar} \right)^2 \right\}^{1/2}$ with $m_{e,h} = \frac{\tilde{m}_{e,h}}{m_0}$, $\tilde{X} = \frac{X}{a_0}$, $\tilde{x} = \frac{x}{a_0}$, $\tilde{a}_e = \frac{a_e}{a_0}$, $\tilde{Z}_{mp} = a_0^2 Z_{mp}$, $\tilde{K}_m = a_0 K_m$, $\tilde{v}_{Fx} = \frac{v_{Fx}}{v_F}$ and $\tilde{E}_m = \frac{E_m 2m_0 a_0^2}{\hbar^2}$ where $\frac{\hbar^2}{2m_0 a_0^2} = E_H = 13.6$ eV is the binding energy of hydrogen atom with the rest mass of electron m_0 and the electron Bohr radius a_0 . These parameters themselves are functions of the semiconducting material where the exciton is formed. For irradiated gapped Kek-Y graphene with parameter $\tilde{\zeta} = 0.1$ at high frequency ($\hbar\Omega = 0.1$ eV), the relevant physical parameters are $m_{e,h} = 8.7 \times 10^{-5} m_0$, $v_{Fx} = 0.208 v_F$, $E_m = \frac{-2 \times 10^{-6}}{(m-1/2)^2} E_H$ and $\tilde{a}_e = \epsilon_b/\tilde{\mu} = 1.14 \times 10^5$ for $\epsilon_b = 4.58$ for hBn. This shows that in the presence of circularly polarized light, Kek-Y graphene supports weakly bound excitons in compared with any other gapped semiconductor because of its very light Dirac particles.⁵²

With these dimensionless parameters, the expressions for the effective potential and two coupled differential equations turn out to be

$$\tilde{Z}_{m,p}(\tilde{X}) = 2\tilde{m}_{e,h} \int_{-\infty}^{\infty} d\tilde{x} \phi_m^*(\tilde{x}) \phi_p(\tilde{x}) \left\{ \tilde{V}_e(\tilde{X} - \tilde{x}/2) + \tilde{V}_h(\tilde{X} + \tilde{x}/2) \right\}, \quad (69)$$

$$\begin{aligned} \frac{dR_{mn}(\tilde{y})}{d\tilde{y}} = & - \sum_{j=0}^{\infty} \frac{1}{2i\tilde{K}'_j} \left\{ e^{i(\tilde{K}'_j - \frac{3\tilde{m}_{e,h}\tilde{v}_{Fx}}{2})\tilde{y}} \delta_{mj} + R_{mj}(\tilde{y}) e^{-i(\tilde{K}'_j - \frac{3\tilde{m}_{e,h}\tilde{v}_{Fx}}{2})\tilde{y}} \right\} \\ & \times \sum_{p=0}^{\infty} \tilde{Z}_{jp}(\tilde{y}) \left\{ e^{i(\tilde{K}'_p - \frac{3\tilde{m}_{e,h}\tilde{v}_{Fx}}{2})\tilde{y}} \delta_{pn} + R_{pn}(\tilde{y}) e^{-i(\tilde{K}'_p - \frac{3\tilde{m}_{e,h}\tilde{v}_{Fx}}{2})\tilde{y}} \right\}, \end{aligned} \quad (70)$$

and

$$\begin{aligned} \frac{dT_{mn}(\tilde{y})}{d\tilde{y}} = & - \sum_{j=0}^{\infty} \frac{1}{2i\tilde{K}'_j} \left\{ e^{i(\tilde{K}'_j - \frac{3\tilde{m}_{e,h}\tilde{v}_{Fx}}{2})\tilde{y}} T_{mj}(\tilde{y}) \right\} \\ & \times \sum_{p=0}^{\infty} \tilde{Z}_{jp}(\tilde{y}) \left\{ e^{i(\tilde{K}'_p - \frac{3\tilde{m}_{e,h}\tilde{v}_{Fx}}{2})\tilde{y}} \delta_{pn} + R_{pn}(\tilde{y}) e^{-i(\tilde{K}'_p - \frac{3\tilde{m}_{e,h}\tilde{v}_{Fx}}{2})\tilde{y}} \right\} \end{aligned} \quad (71)$$

where,

$$\phi_p(\tilde{x}) = N_p \frac{2\tilde{x}}{(p+1)\tilde{a}_e} e^{-|\frac{2\tilde{x}}{(p+1)\tilde{a}_e}|/2} L_{p+1}^1\left(\left|\frac{2\tilde{x}}{(p+1)\tilde{a}_e}\right|\right). \quad (72)$$

First, we consider a square potential barrier V_0 for $0 \leq x_{e,h} \leq d$ and zero otherwise. We plot the center of mass effective potential as a function of center of mass coordinate for equal strength $V_0 = 2 \times E_H$ for electron and hole in Fig. 9(a). It is observed that the effective potential experienced by the center of mass of the exciton is negligible or it almost vanishes and hence perfect transmission is obtained in Fig. 9(b) for finite range of the potential strength. This numerical result can be proved analytically from the expression for effective potential $\tilde{Z}_{m,p}(\tilde{X})$ in Eq. (69), where the effective potential depends not only on the strength of the external barrier but also on the effective mass and the probability that the exciton incident state on the left-hand side of the barrier and on the outgoing state on the right-hand side of the barrier. Since the exciton effective mass is very small $\sim 10^{-5} m_0$ in terms of the free electron rest mass it suppress the integrand transition probability over the potential strength. Therefore, the effective potential comes out to be of order $10^{-7} E_H$ until the potential strength is infinitely large with $V_0 > 10^6$ eV to overcome the role of the effective mass. Hence perfect transmission is observed for the large but finite range of potential strength. It should be mentioned that these numerical results are for barrier width $d = 100 a_0$ which is smaller than the enormously large Bohr radius of an exciton. But for very small effective mass exciton even when the barrier is wider than the exciton Bohr radius the average scalar potential seen by the center of mass is infinitesimally small. Additionally, the probability of transmission of an exciton from one state to another is also destroyed and hence perfect transmission is only allowed between the same eigenstate as if there is no obstacle in the path of propagation of the center of

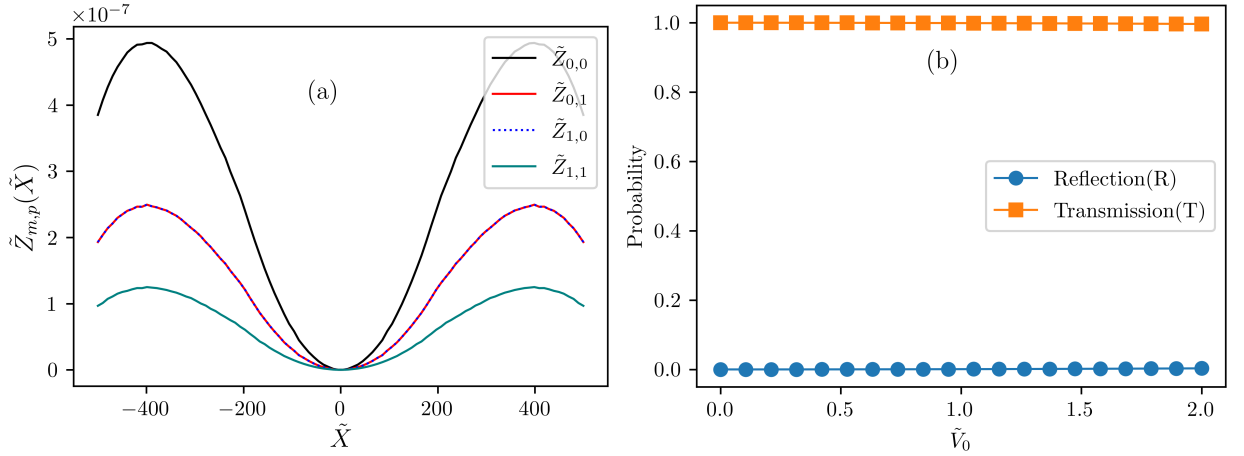


FIG. 9: (Color online) (a) Plot of the effective potential $\tilde{Z}_{m,p}(\tilde{X})$ as a function of the center of mass coordinate \tilde{X} for the center of mass of the exciton when incident in the state p and reflected or transmitted in the state m across a square potential barrier of width d and strength V_0 . (b) Plot of the probability of transmission or reflection of an exciton in state $n = 0$ across a square potential barrier as a function of the strength of the barrier. In the plots, all parameters are dimensionless. We have used $\tilde{m}_{e,h} = 8.7 \times 10^{-5}$ which is for irradiation parameter $\tilde{\zeta} = 0.1$, $\hbar\Omega = 0.1$ eV and $v_F = 10^6$ m/s. Other parameters include $\epsilon_b = 4.58$, $\tilde{a}_e = 2\epsilon_b/\tilde{m}_{e,h}$ and $\tilde{d} = 100$. It is noted that the strengths of the external potential barrier for electron and hole are equal and we have used twice that of the binding energy of the hydrogen atom in (a). In plot (b), the kinetic energy of the exciton is $2 \times 10^{-4} E_H \rightarrow 2.7$ meV and the probability we have plotted is for potential 0 to $10^4 E_y$.

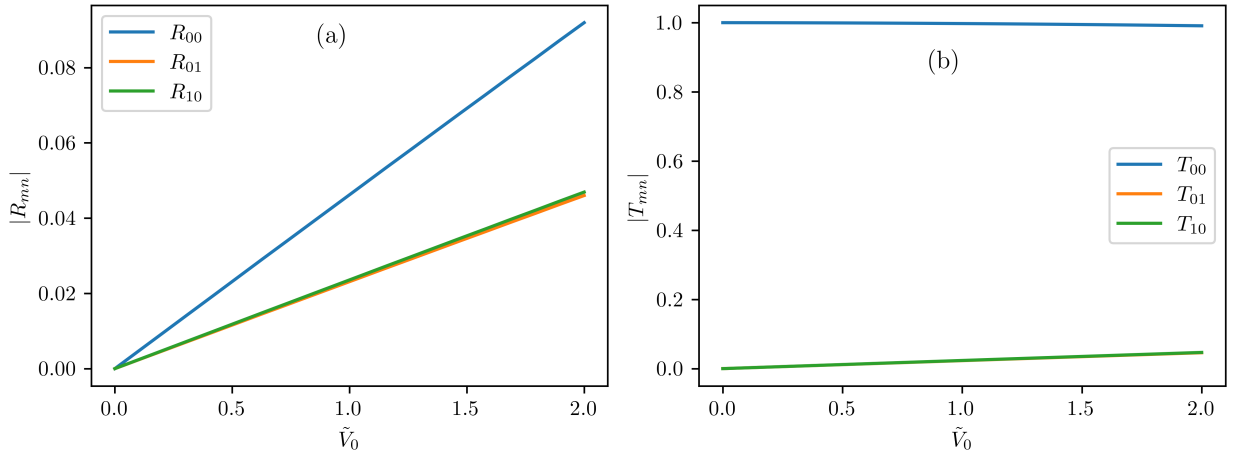


FIG. 10: (Color online) Plot of the probability amplitude for the center of mass of the exciton as a function of the potential height \tilde{V}_0 of a finite width square potential barrier. The exciton is incident in state n and reflected or transmitted in state m . Plot (a) is for the reflection amplitude and plot (b) is for the transmission amplitude. In the plot all parameters are dimensionless. We chose $\tilde{m}_{e,h} = 8.7 \times 10^{-5}$ which is for irradiation parameter $\tilde{\zeta} = 0.1$, $\hbar\Omega = 0.1$ eV and $v_F = 10^6$ m/s. Other parameters include, $\epsilon_b = 4.58$, $\tilde{a}_e = 2\epsilon_b/\tilde{m}_{e,h}$ and $\tilde{d} = 100$. It is noted that the strengths of the external potential barrier for the electron and hole are equal and we chose the exciton kinetic energy as $2 \times 10^{-4} E_H \rightarrow 2.7$ meV and we have plotted the probability for potential 0 to $10^4 E_y$.

mass of an exciton. This conclusion is based on the numerical result presented in Fig. 10, where the amplitude of reflection and transmission between the ground state and the first excited state are plotted as a function of the potential strength. Analytically, it is because the limits of integration for x are symmetric. However, because of orthogonality of the wave functions $\phi_{m,p}(x)$, the integrand is even only when $m = p$. Therefore, the off-diagonal elements are automatically cancelled. From this discussion, it is clear that the effective center of mass potential of a light but enormous Dirac exciton vanishes identically in a scalar barrier of finite height. And hence these excitons incident on a square potential barrier is transmitted to the other side of the barrier without any obstruction.

While discussing these results we have to keep in mind that, the electron-hole quasiparticles are spatially separated

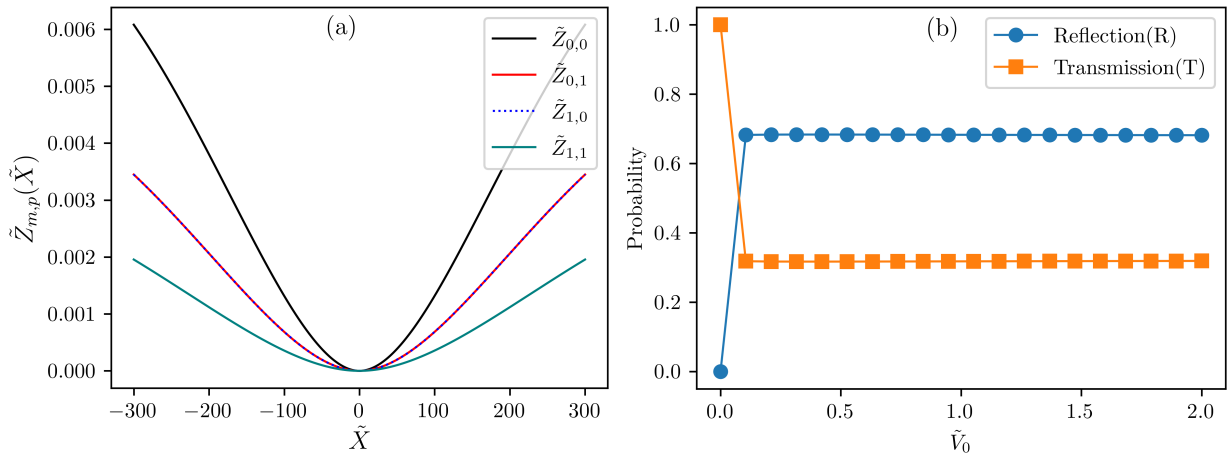


FIG. 11: (Color online) (a) Plot of the effective potential $\tilde{Z}_{m,p}(\tilde{X})$ as a function of the center of mass coordinate \tilde{X} for the center of mass of the exciton when incident in state p and reflected or transmitted in the state m through a delta potential barrier or unequal strength $V_{0,e}$ and $V_{0,h}$, where $V_{0,e} = V_0$ and $V_{0,h} = 10V_0$. (b) Plots of the probability of transmission and reflection of an exciton in state $n = 0$ across a square potential barrier as a function of height of the barrier. In the plots, all parameters are dimensionless. We have chosen $\tilde{m}_{e,h} = 3.5 \times 10^{-3}$ which is for irradiation parameter $\tilde{\zeta} = 0.2$, $\hbar\Omega = 1$ eV and $v_F = 10^6$ m/s. Other parameters include, $\epsilon_b = 4.58$, $\tilde{a} = 2\epsilon_b/\tilde{m}_{e,h}$ and $\tilde{d} = 100$. It is noted that the strength of the delta potential barrier is twice that of the binding energy of the hydrogen atom in (a). In plots (b), the kinetic energy of an exciton is $2 \times 10^{-4} E_H \rightarrow 2.7$ meV and the probability we have plotted for V_0 is 0 to $10^4 E_y$.

in the presence of the externally applied circularly polarized high frequency irradiation. Additionally, the irradiation induced effective mass of electron and holes are equal and can be tuned by manipulating the irradiation parameter but we cannot choose the parameters arbitrarily just to obtain a heavy exciton. We have also assumed that the heights of the external potential barrier for the electron and hole are equal. If one considers the irradiation parameter $\tilde{\zeta}$ high but still less than 1, and the frequency is increased by a factor of 10, the effective mass can be increased by some amount. For the larger effective mass and unequal potential for the electron and hole, the exciton may have finite reflection probability. In Fig. 11, numerical results are presented for effective potential and probabilities when the effective mass of the electron and hole $\tilde{m}_{e,h} = 3.5 \times 10^{-3} m_0$, group velocity $v_{F_x} = 0.416 v_0$ and delta potential of unequal strength for electron and hole given by $V_{e,h}(x) = V_{0,e,h}\delta(x)$. Here, the effective mass and the group velocity are calculated for irradiation parameter $\tilde{\zeta} = 0.2$ and for photon of energy 1 eV.

The results in Fig. 11(a), show that the center of mass of the exciton experienced a very small potential than the individual electron and hole. Additionally, the effective potential depends not only on the strength of the external potential but also the probability for the incident state of the exciton on the left-hand side of the potential and the outgoing state on the right-hand side of the potential. For example, the actual potential seen by the exciton incident in the ground state and transmitted or reflected to the ground state $\tilde{Z}_{0,0}$ is higher than the absolute potential seen by the ground state exciton transmitted or reflected to the first excited state $\tilde{Z}_{1,0}$. Therefore, the exciton in the ground state has higher probability for reflection to the ground state than reflected to the first excited state. It is also seen that the exciton in the ground state and transmitted or reflected to the first excited state have equal effective potential for the exciton in the first excited state transmitted or reflected to the ground state. i.e $\tilde{Z}_{1,0} = \tilde{Z}_{0,1}$. However the total probability of the quasiparticle from ground state cross the potential barrier is the sum of the probability of transmission from ground state to any possible state. The Fig. 11(b) explain that perfect transmission is no longer present when the potential strength of the electron and holes are higher than that of the kinetic energy of the incident exciton. Even the effective potential the center of mass encounters is small it is still greater than the incident kinetic energy of exciton. Therefore quasiparticles are partially transmitted and the transmission probability is constant of potential strength.

VI. CONCLUDING REMARKS

We have investigated the effect due to high frequency irradiation on valley resolved transmission and reflection of charged particles incident on a square potential barrier on monolayer Kek-Y distorted graphene. We employed a low energy Hamiltonian near the Dirac points of Kekulé distorted graphene lattice with Y-shaped bond texture. To

this, we added a high frequency time-dependent perturbation due to external irradiation. We employed the Floquet Magnus expansion to obtain a time independent effective Hamiltonian which has the same stroboscopic effect as the applied time dependent perturbative Hamiltonian for elliptically polarized irradiation. We determined the dressed states and modified energy spectra due to irradiation. The results show that, a dynamical gap between the conduction and valance bands is induced as well as two folded cones are separated by small energy gap at the Dirac point due to circularly polarized irradiation.

After establishing our model Hamiltonian, our next step was to calculate the probability current of transmission and reflection for both undressed and dressed states by solving the continuity equations which apply to the wave functions. Maintaining the translational symmetry along the transverse direction and employing the boundary conditions at the edge of the barrier, an analytical expression for the valley dependent transmission and reflection coefficients were obtained. The presented analytical and numerical results for the transmission probability separating the intervalley and intravalley contributions demonstrates that valley manipulation for the transmission can enhance the Klein tunneling at around normal incidence at small barrier width and suppress resonant tunneling when the barrier becomes wider and wider. Additionally, the electrical conductance is decreased due to opening the new channel (intervalley) for scattering. This suggests that valley degree of freedom can be used in a similar way as spin to control electron transmission through the potential region. Furthermore, highly suppressed transmission probability for irradiated electrons at high frequency, supports the idea that illuminating the material with high frequency electromagnetic field is another effective method for modifying the electronic spectra and controlling the transport properties of graphene. The polar plots for the transmission probability for chosen ratio of irradiation intensity to the frequency, demonstrate that the effect of irradiation is comparatively more significant on intervalley scattering than on the intravalley scattering.

Formation of excitons due to a dynamical gap between electron and hole subbands is another consequence of irradiation which established the ground for the study of the transport properties of such bound quasiparticles in Kek-Y graphene. First, we calculated the electronic spectra of excitons following the one dimensional hydrogenic model and obtained an expression for the effective mass and group velocity of electron and hole in both valleys. The effective mass of an electron and hole in the outer cone is found to be divergent while that for inner cone is equal. As a consequence the intervalley transmission of excitons are not possible in our formalism. Therefore we calculated the reflection and transmission probabilities of an exciton from inner cone incident upon a square potential barrier of equal strength for electron and hole using the numerical method of variable transmission and reflection amplitudes. Our results demonstrate that there is perfect tunneling of an exciton from the ground state of the inner cone through the symmetric potential barrier of finite height irrespective of the height of the barrier as the effective potential experienced by the center of mass of the exciton is insignificantly small in comparison to the potential experienced by the individual electron and hole. Moreover, the even and odd parity coupling between exciton states is forbidden due to the conservation of parity and the symmetry in the Hamiltonian for electron and hole. When a symmetric potential barrier is replaced by a delta potential barrier of unequal strength, the perfect transmission is broken and hence the significant reflection is observed for finite strength of the potential.

In conclusion, high frequency circularly polarized irradiation significantly modifies the electronic spectra and offers more appealing transport phenomena in Kek-Y distorted graphene including suppressed transmission and perfect tunneling of excitons. Another important implication is that these properties can be tuned by varying the values for the intensity and frequency of the irradiation. Our analytical and numerical results correctly reproduce that of unirradiated Kek-Y graphene in the limit of irradiation parameter ζ tends to zero. We believe that our theoretical framework and the numerical analysis are experimentally feasible and these results have their own application in designing and manufacturing the electronic, optoelectronic and valleytronic devices based on graphene.

Acknowledgments

G.G. gratefully acknowledges funding from the U.S. National Aeronautics and Space Administration (NASA) via the NASA-Hunter College Center for Advanced Energy Storage for Space under cooperative agreement 80NSSC24M0177. We also acknowledge support from the Science and Technology Facilities Council (STFC), UK (Reference No. ST/Y005147/1)

Appendix A: Numerical solution of the Transmission coefficient

A lengthy calculation is needed for solving the equations (39) analytically. So, we turn to solving these equations numerically by constructing them in matrix form as, $ML = W$, where M is given by

$$M = \begin{pmatrix} -e^{i\theta_{k+}} & -e^{i\theta_{k-}} & -e^{-i\theta_{q+}} & -e^{-i\theta_{q-}} & e^{i\theta_{q+}} & e^{i\theta_{q-}} & 0 & 0 \\ s & s & -s' & -s' & -s' & -s' & 0 & 0 \\ s & -s & -s' & s' & -s' & s' & 0 & 0 \\ -e^{-i\theta_{k+}} & e^{-i\theta_{k-}} & -e^{i\theta_{q+}} & e^{i\theta_{q-}} & e^{-i\theta_{q+}} & -e^{-i\theta_{q-}} & 0 & 0 \\ 0 & 0 & e^{i(q_x^+ d - \theta_{q+})} & e^{i(q_x^- d - \theta_{q-})} & -e^{-i(q_x^+ d - \theta_{q+})} & -e^{-i(q_x^- d - \theta_{q-})} & -e^{i(k_x^+ d - \theta_{k+})} & -e^{i(k_x^- d - \theta_{k-})} \\ 0 & 0 & s' e^{iq_x^+ d} & s' e^{iq_x^- d} & s' e^{-iq_x^+ d} & s' e^{-iq_x^- d} & -s e^{ik_x^+ d} & -s e^{ik_x^- d} \\ 0 & 0 & s' e^{iq_x^+ d} & -s' e^{iq_x^- d} & s' e^{-iq_x^+ d} & -s' e^{-iq_x^- d} & -s e^{ik_x^+ d} & s e^{ik_x^- d} \\ 0 & 0 & e^{i(q_x^+ d + \theta_{q+})} & -e^{i(q_x^- d + \theta_{q-})} & -e^{-i(q_x^+ d + \theta_{q+})} & -e^{-i(q_x^- d + \theta_{q-})} & -e^{i(k_x^+ d + \theta_{k+})} & e^{i(k_x^- d + \theta_{k-})} \end{pmatrix} \quad (A1)$$

and L and W are column vectors with transpose:

$$L = \begin{pmatrix} r_+ & r_- & \gamma_+ & \gamma_- & \eta_+ & \eta_- & t_+ & t_- \end{pmatrix}^T \quad (A2)$$

$$W = \begin{pmatrix} -e^{-i\theta_{k+}} & -s & -s & -e^{i\theta_{k+}} & 0 & 0 & 0 & 0 \end{pmatrix}^T. \quad (A3)$$

Using Cramer's rule for the j^{th} unknown, $x_j = \det(M_j)/\det(M)$ where M_j is the matrix obtained from M by replacing its j^{th} column by W , We obtained $r_+ = \det(M_1)/\det(M)$, $r_- = \det(M_2)/\det(M)$, $t_+ = \det(M_7)/\det(M)$ and $t_- = \det(M_8)/\det(M)$.

Appendix B: Transmission subjected to irradiation

The reflected and transmitted current from each valley can be expressed as,

$$J_x^{(\tilde{r}_+)} = -2v_F \frac{|\tilde{r}_+|^2}{(1 + b_s^2(\pi - \theta_{k+}))(1 + b_+^2(\pi - \theta_{k+}))} [\cos \theta_{k+} \{b_s(\pi - \theta_{k+})(1 + b_+^2(\pi - \theta_{k+})) + \Delta_0 b_+(\pi - \theta_{k+})(1 + b_s^2(\pi - \theta_{k+}))\} + \tilde{\zeta} \{(1 - b_s^2(\pi - \theta_{k+}))(1 + b_+^2(\pi - \theta_{k+})) + \Delta_0^2(1 + b_s^2(\pi - \theta_{k+}))(1 - b_+^2(\pi - \theta_{k+}))\}], \quad (B1)$$

$$J_x^{(\tilde{r}_-)} = -2v_F \frac{|\tilde{r}_-|^2}{(1 + b_s^2(\pi - \theta_{k-}))(1 + b_-^2(\pi - \theta_{k-}))} [\cos \theta_{k-} \{b_s(\pi - \theta_{k-})(1 + b_-^2(\pi - \theta_{k-})) + \Delta_0 b_-(\pi - \theta_{k-})(1 + b_s^2(\pi - \theta_{k-}))\} + \tilde{\zeta} \{(1 - b_s^2(\pi - \theta_{k-}))(1 + b_-^2(\pi - \theta_{k-})) + \Delta_0^2(1 + b_s^2(\pi - \theta_{k-}))(1 - b_-^2(\pi - \theta_{k-}))\}], \quad (B2)$$

$$J_x^{(\tilde{t}_+)} = 2v_F \frac{|\tilde{t}_+|^2}{(1 + b_s^2(\theta_{k+}))(1 + b_+^2(\theta_{k+}))} [\cos \theta_{k+} \{b_s(\theta_{k+})(1 + b_+^2(\theta_{k+})) + \Delta_0 b_+(\theta_{k+})(1 + b_s^2(\theta_{k+}))\} + \tilde{\zeta} \{(1 - b_s^2(\theta_{k+}))(1 + b_+^2(\theta_{k+})) + \Delta_0^2(1 + b_s^2(\theta_{k+}))(1 - b_+^2(\theta_{k+}))\}], \quad (B3)$$

and

$$J_x^{(\tilde{t}_-)} = 2v_F \frac{|\tilde{t}_-|^2}{(1 + b_s^2(\theta_{k-}))(1 + b_-^2(\theta_{k-}))} [\cos \theta_{k-} \{b_s(\theta_{k-})(1 + b_-^2(\theta_{k-})) + \Delta_0 b_-(\theta_{k-})(1 + b_s^2(\theta_{k-}))\} + \tilde{\zeta} \{(1 - b_s^2(\theta_{k-}))(1 + b_-^2(\theta_{k-})) + \Delta_0^2(1 + b_s^2(\theta_{k-}))(1 - b_-^2(\theta_{k-}))\}], \quad (B4)$$

with the corresponding reflection and transmission wave functions as follows:

$$\Psi_Y^{E(\tilde{r}_+)}(\mathbf{k}; \mathbf{r}) = \frac{\tilde{r}_+}{\sqrt{(1 + b_s^2(\pi - \theta_{k+}))(1 + b_+^2(\pi - \theta_{k+}))}} \begin{pmatrix} -e^{i\theta_{k+}} \\ b_s(\pi - \theta_{k+}) \\ b_+(\pi - \theta_{k+}) \\ -b_s(\pi - \theta_{k+})b_+(\pi - \theta_{k+})e^{-i\theta_{k+}} \end{pmatrix} \frac{e^{ik_y y - i|k_x^+|x}}{\sqrt{A}}, \quad (\text{B5})$$

$$\Psi_Y^{E(\tilde{r}_-)}(\mathbf{k}; \mathbf{r}) = \frac{\tilde{r}_-}{\sqrt{(1 + b_s^2(\pi - \theta_{k-}))(1 + b_-^2(\pi - \theta_{k-}))}} \begin{pmatrix} -e^{i\theta_{k-}} \\ b_s(\pi - \theta_{k-}) \\ b_-(\pi - \theta_{k-}) \\ -b_s(\pi - \theta_{k-})b_-(\pi - \theta_{k-})e^{-i\theta_{k-}} \end{pmatrix} \frac{e^{ik_y y - i|k_x^-|x}}{\sqrt{A}}, \quad (\text{B6})$$

$$\Psi_Y^{E(\tilde{t}_+)}(\mathbf{k}; \mathbf{r}) = \frac{\tilde{t}_+}{\sqrt{(1 + b_s^2(\theta_{k+}))(1 + b_+^2(\theta_{k+}))}} \begin{pmatrix} e^{-i\theta_{k+}} \\ b_s(\theta_{k+}) \\ b_+(\theta_{k+}) \\ b_s(\theta_{k+})b_+(\theta_{k+})e^{i\theta_{k+}} \end{pmatrix} \frac{e^{ik_y y + i|k_x^+|x}}{\sqrt{A}}, \quad (\text{B7})$$

and

$$\Psi_Y^{E(\tilde{t}_-)}(\mathbf{k}; \mathbf{r}) = \frac{\tilde{t}_-}{\sqrt{(1 + b_s^2(\theta_{k-}))(1 + b_-^2(\theta_{k-}))}} \begin{pmatrix} e^{-i\theta_{k-}} \\ b_s(\theta_{k-}) \\ b_-(\theta_{k-}) \\ b_s(\theta_{k-})b_-(\theta_{k-})e^{i\theta_{k-}} \end{pmatrix} \frac{e^{ik_y y + i|k_x^-|x}}{\sqrt{A}}. \quad (\text{B8})$$

In the scattering region (II), the forward moving and backward moving waves are defined as follows,

$$\Psi_Y^{E(\tilde{P}_+)}(\mathbf{k}; \mathbf{r}) = \frac{\tilde{P}_+}{\sqrt{(1 + b_{s'}^2(\theta_{q+}))(1 + b_+^2(\theta_{q+}))}} \begin{pmatrix} e^{-i\theta_{q+}} \\ b_{s'}(\theta_{q+}) \\ b_+(\theta_{q+}) \\ b_{s'}(\theta_{q+})b_+(\theta_{q+})e^{i\theta_{q+}} \end{pmatrix} \frac{e^{ik_y y + i|q_x^+|x}}{\sqrt{A}}, \quad (\text{B9})$$

$$\Psi_Y^{E(\tilde{P}_-)}(\mathbf{k}; \mathbf{r}) = \frac{\tilde{P}_-}{\sqrt{(1 + b_{s'}^2(\theta_{q-}))(1 + b_-^2(\theta_{q-}))}} \begin{pmatrix} e^{-i\theta_{q-}} \\ b_{s'}(\theta_{q-}) \\ b_-(\theta_{q-}) \\ b_{s'}(\theta_{q-})b_-(\theta_{q-})e^{i\theta_{q-}} \end{pmatrix} \frac{e^{ik_y y + i|q_x^-|x}}{\sqrt{A}}, \quad (\text{B10})$$

$$\Psi_Y^{E(\tilde{Q}_+)}(\mathbf{k}; \mathbf{r}) = \frac{\tilde{Q}_+}{\sqrt{(1 + b_{s'}^2(\pi - \theta_{q+}))(1 + b_+^2(\pi - \theta_{q+}))}} \begin{pmatrix} -e^{i\theta_{q+}} \\ b_{s'}(\pi - \theta_{q+}) \\ b_+(\pi - \theta_{q+}) \\ -b_{s'}(\pi - \theta_{q+})b_+(\pi - \theta_{q+})e^{-i\theta_{q+}} \end{pmatrix} \frac{e^{ik_y y - i|q_x^+|x}}{\sqrt{A}}, \quad (\text{B11})$$

and

$$\Psi_Y^{E(\tilde{Q}_-)}(\mathbf{k}; \mathbf{r}) = \frac{\tilde{Q}_-}{\sqrt{(1 + b_{s'}^2(\pi - \theta_{q-}))(1 + b_-^2(\pi - \theta_{q-}))}} \begin{pmatrix} -e^{i\theta_{q-}} \\ b_{s'}(\pi - \theta_{q-}) \\ b_-(\pi - \theta_{q-}) \\ -b_{s'}(\pi - \theta_{q-})b_-(\pi - \theta_{q-})e^{-i\theta_{q-}} \end{pmatrix} \frac{e^{ik_y y - i|q_x^-|x}}{\sqrt{A}}, \quad (\text{B12})$$

where \tilde{P}^τ and \tilde{Q}^τ are the coefficient of forward moving and backward moving particles, $q_\tau = \frac{\varepsilon_Y^E - V_0}{s' \hbar v_F [(1 + \tau \Delta_0) + 2\zeta^2 \cos^2 \theta_{q^\tau} (1 + \tau \Delta_0^3)]}$, $q_x^\tau = q_\tau \cos \theta_{q^\tau}$, $k_y = k_\tau \sin \theta_{k^\tau}$ and $s' = \text{sign}(\varepsilon_Y^E - V_0)$.

Using the continuity condition for the wave functions at $x = 0$ and at $x = d$, we obtain eight simultaneous equations for eight unknowns, i.e., $\tilde{r}_+, \tilde{r}_-, \tilde{t}_+, \tilde{t}_-, \tilde{P}_+, \tilde{P}_-, \tilde{Q}_+, \tilde{Q}_-$, so that $\tilde{M} \tilde{L} = \tilde{W}$ where,

$$\tilde{M} = \begin{pmatrix} \tilde{M}_{11} & \tilde{M}_{12} & \cdots & \tilde{M}_{18} \\ \tilde{M}_{21} & \tilde{M}_{22} & \cdots & \tilde{M}_{28} \\ \vdots & \vdots & \ddots & \vdots \\ \tilde{M}_{81} & \tilde{M}_{82} & \cdots & \tilde{M}_{88} \end{pmatrix}$$

$$M_{ij} = f(i, j, \theta, V, k) \quad \text{for } i, j = 1, \dots, 8$$

$$M = (M_{ij})_{8 \times 8}$$

$$\tilde{L} = \left(\tilde{r}_+ \ \tilde{r}_- \ \tilde{P}_+ \ \tilde{P}_- \ \tilde{Q}_+ \ \tilde{Q}_- \ \tilde{t}_+ \ \tilde{t}_- \right)^T \quad (\text{B13})$$

and

$$\tilde{W} = \frac{1}{N_i} \left(-e^{-i\theta_{k^+}} \ -b_s(\theta_{k^+}) \ -b_+(\theta_{k^+}) \ -b_s(\theta_{k^+})b_+(\theta_{k^+})e^{i\theta_{k^+}} \ 0 \ 0 \ 0 \ 0 \right)^T. \quad (\text{B14})$$

We follow the same procedure as we did in the absence of irradiation to solve for the unknowns $\tilde{r}_+, \tilde{r}_-, \tilde{t}_+, \tilde{t}_-$ from the matrix equation $\tilde{M} \tilde{L} = \tilde{W}$. We have

$$\alpha = \frac{(1 + b_s^2(\theta_{k^+}))(1 + b_+^2(\theta_{k^+}))}{(1 + b_s^2(\theta_{k^-}))(1 + b_-^2(\theta_{k^-}))} \begin{bmatrix} \cos \theta_{k^-} \{b_s(\theta_{k^-})(1 + b_-^2(\theta_{k^-})) + \Delta_0 b_-(\theta_{k^-})(1 + b_s^2(\theta_{k^-}))\} + \\ \tilde{\zeta} \{(1 - b_s^2(\theta_{k^-}))(1 + b_-^2(\theta_{k^-})) + \Delta_0^2(1 + b_s^2(\theta_{k^-}))(1 - b_-^2(\theta_{k^-}))\} \\ \cos \theta_{k^+} \{b_s(\theta_{k^+})(1 + b_+^2(\theta_{k^+})) + \Delta_0 b_+(\theta_{k^+})(1 + b_s^2(\theta_{k^+}))\} + \\ \tilde{\zeta} \{(1 - b_s^2(\theta_{k^+}))(1 + b_+^2(\theta_{k^+})) + \Delta_0^2(1 + b_s^2(\theta_{k^+}))(1 - b_+^2(\theta_{k^+}))\} \end{bmatrix} \quad (\text{B15})$$

$$\Lambda = \frac{(1 + b_s^2(\theta_{k^+}))(1 + b_+^2(\theta_{k^+}))}{(1 + b_s^2(\pi - \theta_{k^+}))(1 + b_+^2(\pi - \theta_{k^+}))} \begin{bmatrix} \cos \theta_{k^+} \{b_s(\pi - \theta_{k^+})(1 + b_+^2(\pi - \theta_{k^+})) + \Delta_0 b_+(\pi - \theta_{k^+}) \times \\ (1 + b_s^2(\pi - \theta_{k^+}))\} - \tilde{\zeta} \{(1 - b_s^2(\pi - \theta_{k^+}))(1 + b_+^2(\pi - \theta_{k^+}))\} \\ + \Delta_0^2(1 + b_s^2(\pi - \theta_{k^+}))(1 - b_+^2(\pi - \theta_{k^+}))\} \\ \cos \theta_{k^+} \{b_s(\theta_{k^+})(1 + b_+^2(\theta_{k^+})) + \Delta_0 b_+(\theta_{k^+})(1 + b_s^2(\theta_{k^+}))\} + \\ \tilde{\zeta} \{(1 - b_s^2(\theta_{k^+}))(1 + b_+^2(\theta_{k^+})) + \Delta_0^2(1 + b_s^2(\theta_{k^+}))(1 - b_+^2(\theta_{k^+}))\} \end{bmatrix} \quad (\text{B16})$$

and

$$\kappa = \frac{(1 + b_s^2(\theta_{k^+}))(1 + b_+^2(\theta_{k^+}))}{(1 + b_s^2(\pi - \theta_{k^-}))(1 + b_-^2(\pi - \theta_{k^-}))} \begin{bmatrix} \cos \theta_{k^-} \{b_s(\pi - \theta_{k^-})(1 + b_-^2(\pi - \theta_{k^-})) + \Delta_0 b_-(\pi - \theta_{k^-}) \times \\ (1 + b_s^2(\pi - \theta_{k^-}))\} - \tilde{\zeta} \{(1 - b_s^2(\pi - \theta_{k^-}))(1 + b_-^2(\pi - \theta_{k^-}))\} \\ + \Delta_0^2(1 + b_s^2(\pi - \theta_{k^-}))(1 - b_-^2(\pi - \theta_{k^-}))\} \\ \cos \theta_{k^+} \{b_s(\theta_{k^+})(1 + b_+^2(\theta_{k^+})) + \Delta_0 b_+(\theta_{k^+})(1 + b_s^2(\theta_{k^+}))\} + \\ \tilde{\zeta} \{(1 - b_s^2(\theta_{k^+}))(1 + b_+^2(\theta_{k^+})) + \Delta_0^2(1 + b_s^2(\theta_{k^+}))(1 - b_+^2(\theta_{k^+}))\} \end{bmatrix} \quad (\text{B17})$$

¹ D. Aggarwal , R. Narula, and S. Ghosh, Moire fractals in twisted graphene layers, *Phys. Rev. B* **109**, 125302 (2024).

² R. Bistritzer and A. H. MacDonald, Moiré butterflies in twisted bilayer graphene, *Phys. Rev. B* **84**, 035440 (2011).

³ G. G. Naumis, S. Barraza-Lopez, M. Oliva-Leyva, and H. Terrones, Electronic and optical properties of strained graphene and other strained 2D materials: a review, *Rep. Prog. Phys.* **80**, 096501 (2017).

⁴ Y. Liao, C. Song, Y. Xiang, and X. Dai, Recent Advances in Spatial Self-Phase Modulation with 2D Materials and its Applications, *Physik* **532**, 2000322 (2020). <https://doi.org/10.1002/andp.202000322>

⁵ Po-Hsin Shih, Thi-Nga Do, G. Gumbs and Ming-Fa Lin, Electronic and optical properties of doped graphene, *Physica E: Low-Dimensional Systems and Nanostructures*, **118**, 113894 (2020).

⁶ Z. Peng, X. Chen, Y. Fan, D. J. Srolovitz and D. Lei, Strain engineering of 2D semiconductors and graphene: from strain fields to band-structure tuning and photonic applications, *Light Sci. Appl.* **9**, 190 (2020). <https://doi.org/10.1038/s41377-020-00421-5>

⁷ E. Andrade, R. Carrillo-Bastos, and G. G. Naumis, Valley engineering by strain in Kekulé-distorted graphene, *Phys. Rev. B* **99**, 035411 (2019).

⁸ O. V. Gamayun, V. P. Ostroukh, N. V. Gnezdilov, I. Adagideli, and C. W. J. Beenakker, Valley-momentum locking in a graphene superlattice with y-shaped Kekulé bond texture, *New J. Phys.* **20**, 023016 (2018).

⁹ E. Andrade, R. Carrillo-Bastos and G. G. Naumis, Topical review: electronic and optical properties of Kekulé and other short wavelength spatial modulated textures of graphene, *J. Phys.: Condens. Matter* **37** 193003 (2025)

¹⁰ S. A. Herrera and G. G. Naumis, Dynamic polarization and plasmons in Kekulé-patterned graphene: Signatures of broken valley degeneracy, *Phys. Rev. B* **102**, 205429 (2020).

¹¹ M. A. Mojarrro , V. G. Ibarra-Sierra , J. C. Sandoval-Santana , R. Carrillo-Bastos , and Gerardo G. Naumis, Dynamical Floquet spectrum of Kekulé-distorted graphene under normal incidence of electromagnetic radiation, *Phys. Rev. B* **102**, 165301 (2020). DOI: <https://doi.org/10.1103/PhysRevB.102.165301>

¹² S. A. Herrera and G. G. Naumis, Electronic and optical conductivity of Kekulé-patterned graphene: Intravalley and inter-valley transport, *Phys. Rev. B* **101**, 205413 (2020).

¹³ C. Bao , H. Zhang , T. Zhang , Xi Wu, L. Luo, S. Zhou, Q. Li, Y. Hou, W. Yao , L. Liu , Pu Yu , J. Li, W. Duan, H. Yao, Y. Wang , and S. Zhou, Experimental Evidence of Chiral Symmetry Breaking in Kekulé-Ordered Graphene, *Phys. Rev. Lett.* **126**, 206804 (2021).

¹⁴ C. Gutie rrez, C.-J. Kim, L. Brown, T. Schiros, D. Nordlund, E. Lochocki, K. M. Shen, J. Park, and A. N. Pasupathy, Imaging chiral symmetry breaking from Kekulé bond order in graphene, *Nat. Phys.* **12**, 950 (2016).

¹⁵ D. Eom and J.-Y. Koo, Direct measurement of strain-driven Kekulé distortion in graphene and its electronic properties, *Nanoscale* **12**, 19604 (2020).

¹⁶ J. J. Wang, S. Liu, J. Wang, and J.-F. Liu, Valley-coupled transport in graphene with Y-shaped Kekulé structure, *Phys. Rev. B* **98**, 195436 (2018).

¹⁷ L. Gonza lez-A rraga, F. Guinea, and P. San-Jose, Modulation of Kekulé adatom ordering due to strain in graphene *Phys. Rev. B* **97**, 165430 (2018).

¹⁸ E. Andrade, R. Carrillo-Bastos, P. A. Pantaleón, and F. Mireles, Resonant transport in Kekulé-distorted graphene nanoribbons, *J. Appl. Phys.* **127**, 054304 (2020).

¹⁹ Q.-P. Wu, L.-L. Chang, Y.-Z. Li, Z.-F. Liu, and X.-B. Xiao, Electric-Controlled Valley Pseudo magneto resistance in Graphene with Y-Shaped Kekulé Lattice Distortion, *Nanoscale Res. Lett.* **15**, 1 (2020).

²⁰ Y. Mohammadi and S. Bahrami, Integer quantum Hall effect in Kekulé-patterned graphene, *Chin. Phys. B* **31** 017305 (2022). DOI: [10.1088/1674-1056/ac1b82](https://doi.org/10.1088/1674-1056/ac1b82)

²¹ Z. Tajkov, J. Koltai, J. Cserti, and L. Oroszlány, Competition of topological and topologically trivial phases in patterned graphene based heterostructures, *Phys. Rev. B* **101**, 235146 (2020).

²² Y. Liu, C.-S. Lian, Y. Li, Y. Xu, and W. Duan, Pseudospins and Topological Effects of Phonons in a Kekulé Lattice, *Phys. Rev. Lett.* **119**, 255901 (2017).

²³ P. A. Pantaleón, R. Carrillo-Bastos, and Y. Xian, Topological magnon insulator with a Kekulé bond modulation, *J. Phys.: Condens. Matt.* **31**, 085802 (2019).

²⁴ C. Moulsdale, P. A. Pantaleón, R. Carrillo-Bastos, and Y. Xian, Unconventional thermal magnon Hall effect in a ferromagnetic topological insulator, *Phys. Rev. B* **99**, 214424 (2019).

²⁵ O. V. Kibis, I. V. Iorsh and I. A. Shelykh, Floquet engineering of 2D materials, *J. Phys.: Conf. Ser.* **1461** 012064, (2020). DOI 10.1088/1742-6596/1461/1/012064

²⁶ A. Iurov, G. Gumbs, D. Huang, Exchange and correlation energies in silicene illuminated by circularly polarized light, *J. of Mod. Opt.* **64** , 913-920 (2017).

²⁷ A. Iurov, L. Zhemchuzhna, G. Gumbs, D. Huang, W.-K. Tse, K. Blaise and C. Ejiogu , Floquet engineering of tilted and gapped Dirac bandstructure in 1T'-MoS₂, *Sci. Rep.* **12**, 21348 (2022). <https://doi.org/10.1038/s41598-022-25898-5>

²⁸ J.-Yi Zhu, Z.-Rong Liu , R. Chen and B. Zhou, Floquet-induced two-dimensional weak topological insulator phase, *Phys. Rev. B* **112**, 115436 (2025). DOI: <https://doi.org/10.1103/kqly-w5d3>

²⁹ A. Castro, U. De Giovannini, S. A. Sato, H. Hubener and A. Rubio, Floquet engineering the band structure of materials with optimal control theory, *Phys. Rev. Research* **4**, 033213 (2022). DOI: <https://doi.org/10.1103/PhysRevResearch.4.033213>

³⁰ Y. Kobayashi, C. Heide, A.C. Johnson, V. Tiwari, F. Liu, D. A. Reis, T. F. Heinz, and S. Ghimire, Floquet engineering of strongly driven excitons in monolayer tungsten disulfide, *Nat. Phys.* **19**, 171–176 (2023). <https://doi.org/10.1038/s41567-023-02000-0>

022-01849-9

³¹ M. V. Fistul and K. B. Efetov, Electromagnetic-Field-Induced Suppression of Transport through *n-p* Junctions in Graphene, Phys. Rev. Lett. **98**, 256803 (2007).

³² S. V. Syzranov, M. V. Fistul, and K. B. Efetov, Effect of radiation on transport in graphene, Phys. Rev. B **78**, 045407 (2008).

³³ Oka, T. and Aoki, H. Photovoltaic Hall effect in graphene. Phys. Rev. B **79**, 081406 (2009).

³⁴ M. Merboldt, M. Schuler, D. Schmitt, J. P. Bange, W. Bennecke, K. Gadge, K. Pierz, H. W. Schumacher, D. Momeni, D. Steil et.al., Observation of Floquet states in graphene, Nat. Phys., **21** 1093-1099 (2025).

³⁵ B. N. Zakhariev and S. N. Sokolov, Intensified Tunnel Effect for Complex Particles, Ann. Phys. **469**, 229 (1964). <https://doi.org/10.1002/andp.19644690502> Digital Object Identifier (DOI)

³⁶ I. Amirkhanov and B. N. Zakhariev, Violation of barrier penetration symmetry for composite particles, Sov. Phys. JETP, **22**, 764 (1966).

³⁷ N. Saito and Y. Kayanuma, Resonant tunnelling of a composite particle through a single potential barrier, J. Phys. Cond. Matt. **6**, 3759 (1994).

³⁸ J. J. Kavka, D. Kerbrat, and M. R. A. Shegelski, Quantum tunneling and reflection of a molecule with a single bound state, Phys. Rev. A **81**, 022708 (2010).

³⁹ J. J. Kavka, M. R. A. Shegelski and W.-P. Hong, Tunneling and reflection of an exciton incident upon a quantum heterostructure barrier, J. Phys.: Cond. Matt. **24** 365802 (2012).

⁴⁰ M. R. A. Shegelski, J. Pittman, R. Vogt, J. J. Kavka and M. Mandy, Tunnelling of a molecule with many bound states in three dimensions, J. Phys. B: At. Mol. Opt. Phys. **46** 045201 (2013).

⁴¹ L. Wang , S. Papadopoulos, F. Iyikanat , J. Zhang, J. Huang , T. Taniguchi, K. Watanabe, M. Calame , M. L. Perrin , F. Javier, G. de Abajo and L. Novotny, Exciton-assisted electron tunnelling in van der Waals heterostructures, Nat. Materials (2023). <https://doi.org/10.1038/s41563-023-01556-7>

⁴² H. Cao, G. Klimovitch, G. Björk, and Y. Yamamoto, Direct creation of quantum well excitons by electron resonant tunneling, Phys. Rev. Lett. **75**, 1146–1149 (1995).

⁴³ S. M. Cao, and M. Willander, Exciton-induced tunneling effect on the current-voltage characteristics of resonant tunneling diodes, J. Appl. Phys. **81**, 6221–6228 (1997).

⁴⁴ A. Iurov, L. Zhemchuzhna, G. Gumb, and D. Huang, Application of WKB theory to investigating the electron tunneling in Kek-Y graphene, App. Sci. **13**, 6095 (2023).

⁴⁵ M. I. Katsnelson, K. S. Novoselov and A. K. Geim, Chiral tunnelling and the Klein paradox in graphene, Nat. Phys. **2** 620 (2006).

⁴⁶ P. E. Allain and J. N. Fuchs, Klein tunneling in graphene : Optics with massless electrons, Eur. Phys. J. B **83** 301-317 (2011).

⁴⁷ D. Dahal and G. Gumb, Effect of energy band gap in graphene on negative refraction through the veselago lens and electron conductance, Journal of Physics and Chemistry of Solids **100** 83-91 (2017)

⁴⁸ Y. Betancur-Ocampo, G. Monsivais, and V. Jakubsky, Topical Review: The rise of Klein tunneling in low-dimensional materials and superlattices, (preprint, 10.13140/RG.2.2.28280.71684.), (2026)

⁴⁹ M.I. Katsnelson, Zitterbewegung, chirality, and minimal conductivity in graphene, The Eur. Phys. J. B **51**, 157–160 (2006). DOI: 10.1140/epjb/e2006-00203-1

⁵⁰ S. Kandel, G. Gumb, T. Lee, and O. L. Berman, Tuning excitons and superfluidity of dipolar excitons in double layers of kagome lattice by applying circularly polarized irradiation, Phys. Rev. B **112**, 195424 (2025).

⁵¹ M. Razavy, Quantum Theory of Tunneling (Singapore: World Scientific) (2003).

⁵² Ioffe Institute, Physical Properties of Gallium Arsenide(GaAs), WWW Document, www.ioffe.ru/SVA/NSM/Semicond/GaAs.